Journal of Materials Chemistry A

REVIEW

View Article Online
View Journal | View Issue

Cite this: J. Mater. Chem. A, 2024, 12, 33427

A review of detecting Li plating on graphite anodes based on electrochemical methods

Ruoxuan Chen,†[a] Sicheng Miao,†[a] Ye Jia,[a] Xuemei Zhang,[a] Jianan Peng,[a] Kailong Zhang,[b] Fanglin Wu,[c] Jiangqi Zhao,[a] Zeheng Li*[d] and Wenlong Cai*[a]

Received 21st August 2024
Accepted 31st October 2024

DOI: 10.1039/d4ta05871b

rsc.li/materials-a

Lithium plating, a highly detrimental process in lithium-ion batteries (LIBs), accelerates battery aging and induces rapid battery performance decline. Under extreme conditions, lithium plating can even compromise safety performance and lead to thermal runaway combustion and other consequences. Therefore, it is of great significance to detect and understand the internal mechanism of lithium plating. Electrochemical methods stand out among various detection approaches due to their convenience. In this review, we first discuss the formation mechanism of lithium plating metal and then introduce the corresponding detection methods by various electrochemical methods. Finally, we provide some prospects for future research on electrochemical detection methods for lithium plating.

1 Introduction

The looming set of climate change issues requires immediate global implementation of a shift from fossil fuel energy to clean renewable energy.[1–8] Many countries aim for net-zero emissions by 2050 to fulfill the Paris Agreement, which will be achieved through a massive expansion of renewable energy production.[9–15] In recent years, lithium-ion batteries (LIBs) have been widely used as energy storage devices in many industrial sectors, including electric vehicles and grid facilities,[15–22] due to their excellent energy and power densities, high energy efficiency, and long cycle life.[23–31]

At present, graphite stands as the predominant anode material for LIBs due to its good electrical conductivity, low cost, low lithiation potential, good thermal conductivity, high coulombic efficiency (CE), and stable structure.[32–40] Nevertheless, due to the layered structure and anisotropy, lithium ions can only be embedded at the edge of graphite, resulting in low mass transfer efficiency and high propensity for lithium plating, which is an unsavory side effect on the anode side of LIBs that tends to occur during charging at low temperatures, high C rates, or high cut-off voltages.[41–44] Lithium plating results from lithium ions being reduced to lithium metal instead of being intercalated into the anode crystal structure when the local anode potential drops below 0 V *vs.* Li^+/Li.[45,46] The development of lithium metal formation triggers the thickening of the SEI layer, subsequently depleting the limited electrolyte and lithium ions. This process, on the one hand, alters the battery's internal impedance. Primarily, the thickening of the SEI layer caused by lithium plating increases the interface impedance. Additionally, because the electrical conductivity of lithium metal is better than that of graphite, the charge transfer impedance will be correspondingly reduced after lithium plating. On the other hand, this process results in a loss of lithium inventory and loss of anode active material, ultimately accelerating the capacity degradation of the battery.[47] Furthermore, under certain extreme conditions, the growth of lithium dendrites can puncture the separator, leading to thermal runaway.[23] At present, the main strategies to inhibit lithium plating include electrolyte design,[48–52] material modification,[53,54] and optimization of charging protocols.[55–61] These strategies target various rate-limiting steps associated with lithium-ion transportation including lithium-ion migration in the electrolyte, and lithium-ion diffusion in the solid electrolyte interphase (SEI) and graphite.[62] However, in practical applications, the complex interplay between test conditions like rate, state of charge (SOC), and temperature makes it difficult for a single rate-limiting step to remain continuously functioning throughout the entire process, limiting the effectiveness of these strategies in preventing lithium plating.[63] Therefore, it is necessary to develop reliable methods for *in situ*, real-time detection of lithium plating in lithium batteries.

The current methods for detecting lithium plating can be roughly divided into two categories: destructive and non-destructive methods. The former includes (a) visual observation,[41] (b) destructive physical analysis of the battery,[64–66] (c) electron paramagnetic resonance (EPR) and nuclear magnetic

[a]Department of Advanced Energy Materials, College of Materials Science and Engineering, Sichuan University, Chengdu, 610064, China. E-mail: caiwl@scu.edu.cn
[b]School of Chemical Engineering, Huaiyin Institute of Technology, Huaian, 223003, China
[c]State Key Laboratory of Advanced Technology for Materials Synthesis and Processing, Wuhan University of Technology, Wuhan, 430070, China
[d]College of Chemical and Biological Engineering, Zhejiang University, Hangzhou, 310027, China. E-mail: zehengli@zju.edu.cn
† These authors contributed equally to this work.

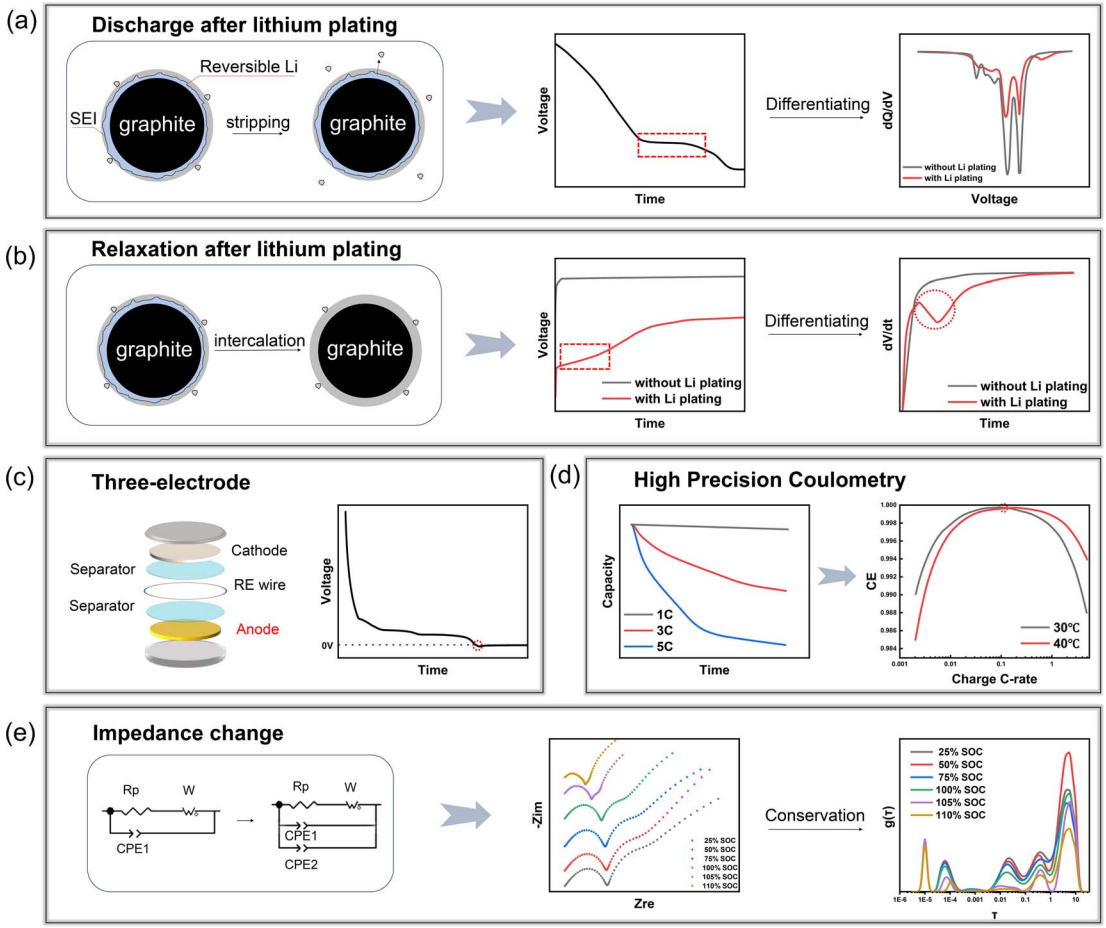

Fig. 1 Electrochemical test methods for analyzing lithium plating. (a) Changes of graphite during discharging, voltage curve, and dQ/dV curve. (b) Changes of graphite during relaxation (rest after charging), voltage curve, and dV/dt curve. (c) Three-electrode device and voltage curve. (d) Capacity fading during cycling and CE changes with charging C rate. (e) Change of equivalent circuit after lithium plating, EIS, and distribution of relaxation times (DRT).

resonance (NMR),[67] and (d) mass spectrometry titration,[68] while the non-destructive methods include (i) battery thickness measurements,[69,70] (ii) *in situ* neutron diffraction,[71] (iii) acoustic detection,[72–74] and (iv) thermal signature detection.[75–77] These different kinds of methods can detect lithium plating and can provide information on lithium plating from different dimensions, but the destructive methods usually require heavy additional equipment or need to be detected after disassembling the battery, while the routine non-destructive methods also have drawbacks in that they are less sensitive to lithium plating. Among the non-destructive methods, electrochemical detection stands out for its simplicity and high sensitivity to lithium plating, eliminating the need for battery disassembly, complex sample preparation, and additional detection equipment.[23,41,45,66,78] However, previous work often utilized only one or two electrochemical detection methods without providing a clear explanation of the detection principle or a systematic study of these methods. In this review, we first analyze the mechanism of lithium plating, and systematically introduce various corresponding electrochemical methods in detail, including three-electrode detection of anode voltage, electrochemical impedance spectroscopy (EIS), detection of the voltage platform during discharging or relaxation, and analysis of CE changes (Fig. 1). Finally, we present the suggestions and prospects for the future development of electrochemical detection methods for lithium electroplating.

2 Lithium plating in LIBs

Under ideal normal charging conditions, lithium ions de-intercalate from the cathode, shuttle to the anode through the electrolyte and separator, and rapidly intercalate into the active material of the anode (commonly graphite).[79–81] However, the equilibrium electrode potential of graphite is close to the potential of lithium metal, which leads to its susceptibility of being reduced to a silvery-white lithium metal on the surface.[82] The occurrence of lithium plating is influenced by many factors, and the following are some of them: (1) high charging rate;[83–85] (2) low temperature;[83,86–88] (3) high SOC;[89,90] (4) long-term cycling.[91]

In either case, the underlying mechanism for lithium plating is poor anode kinetics, whereby the rate of intercalation of

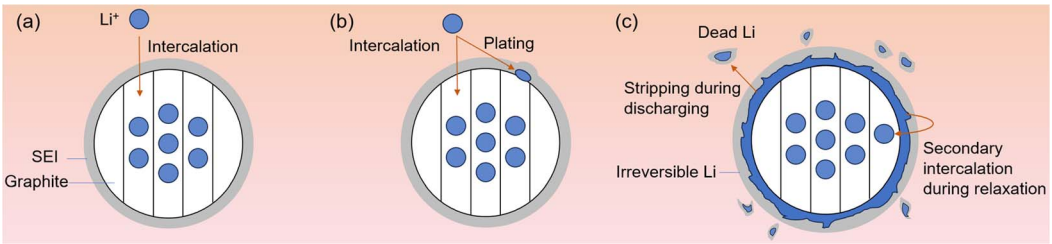

Fig. 2 (a) Intercalation of Li^+ into graphite. (b) Lithium plating phenomenon. (c) The stripping of lithium and the re-insertion of reversible lithium is accompanied by the emergence of dead lithium and the formation of a new SEI.

lithium ions into the graphite interior is slower than the rate of aggregation on the graphite electrode's surface, leaving the graphite anode with an operating potential below 0 V (*vs.* Li^+/Li), which ultimately leads to lithium plating. However, in actual processes, lithium plating does not occur as soon as the voltage drops below 0 V. Due to the existence of certain energy barriers for the formation of lithium metal on the surface of graphite, there is an overpotential below which lithium plating takes place.[13] And the process of lithium plating occurs in multiple steps. As shown in eqn (1), lithium ions de-intercalate from the cathode under ideal normal charging conditions and fully intercalate inside the graphite anode (Fig. 2a). As the charging process continues, lithium ions continue to be intercalated into the graphite anode, and the vacancy sites in the graphite layer decrease, resulting in the anode being in a high SOC. Under this circumstance, as shown in Fig. 2b, the aggregation rate of lithium ions on the anode surface is faster than the intercalating rate, leading to a decrease of the anode potential to below 0 V, which makes lithium plating thermodynamically amenable, indicating lithium plating is initiated (eqn (2)). In theory, the lithium plating process also exists simultaneously with the lithium intercalation process.

$$x\mathrm{Li}^+ + \mathrm{Li}_\alpha\mathrm{C}_6 + x\mathrm{e}^- \rightarrow \mathrm{Li}_{\alpha+x}\mathrm{C}_6 \quad (1)$$

$$z\mathrm{Li}^+ + z\mathrm{e}^- \rightarrow z\mathrm{Li} \quad (2)$$

The plated lithium in the lithium plating process can generally be divided into two categories, namely "live lithium" and "dead lithium." As shown in Fig. 2c, "live lithium" refers to reversible plated lithium, which can be converted into lithium ions to be released into the electrolyte and transferred to the cathode in the subsequent discharging stage after charging, a process known as lithium stripping (eqn (3)).[92,93] Interestingly, a portion of the live lithium can also be re-intercalated into graphite during deposition and relaxation, as shown in eqn (4).[94,95]

$$\mathrm{Li}_\beta \rightarrow \mathrm{Li}^+ + \mathrm{e}^- \quad (3)$$

$$\sigma\mathrm{Li}_\beta + \mathrm{Li}_{\alpha+x}\mathrm{C}_6 \rightarrow \mathrm{Li}_{\alpha+x+\sigma}\mathrm{C}_6 \quad (4)$$

where Li_β is reversible lithium.

Dead lithium is irreversible lithium, where a portion of the plated lithium reacts with the electrolyte to form a new SEI that loses electrical contact with the graphite anode and the conducting collector (Fig. 2c).[96–98] This part of the plated lithium cannot return to the system during the simple lithium stripping process, which can lead to the capacity degradation of LIBs. With the accumulation of dead lithium, the capacity and other aspects of the performance of batteries would further decline.[98–102] In addition, with the emergence of lithium plating, dendrites will form and grow to pierce the separator, resulting in an internal short circuit. Once a short circuit occurs in the battery, its internal heat release will cause the organic electrolyte to burn and cause serious safety accidents.[100,103–107] Therefore, reliable electrochemical methods of detecting lithium plating can be a powerful predictor of the occurrence of these phenomena to ensure safe battery operation.[80,108–112]

3 Electrochemical methods for lithium plating detection

Advanced lithium plating detection methods are rapidly evolving,[41] such as (1) chemical methods focusing on elemental/valence detection and morphological studies,[68] (2) thermal methods using thermal signature detection and analysis such as dT/dt, dT/dQ, dT/dV, or calorimetry,[75–77] and (3) physical methods employing perturbation by electrons, pressure, acoustic waves, or ultrasonic waves to generate relevant information for lithium plating detection.[69,70] For example, estimating exhaust gases using mass spectrometric titration is a precise quantitative technique for detecting inactive lithium in trace amounts of graphite.[23] And microscopic observation of lithium plating typically requires the utilization of optical microscopy, scanning electron microscopy (SEM), and transmission electron microscopy (TEM). These characterization methods play an important role in observing dendritic lithium from the millimeter to nanometer scale.[45] While these methods provide a lot of useful information, they usually require bulky additional equipment or invasive probes inside the cell, and many of the methods are not capable of *in situ* detection.[113] These limitations restrict their practical applications. In contrast to these methods, electrochemical methods have the distinct advantage of detecting lithium without the need for external sensors or equipment, and do not require expensive laboratory-grade instrumentation and meticulous sample preparation.[41] In this chapter, based on the accuracy of tests, detailed information about the electrochemical methods for

detecting lithium plating is introduced. The methods are discussed in terms of their principle, advantages, disadvantages, and specific points to consider.

3.1 Common methods

In electrochemical detection characterization, the most commonly used method is based on the lithium plated on the graphite surface during the charging process and analyzing the voltage change or the amount based on the change in voltage during discharging or relaxation to detect whether lithium plating occurs. These methods are the simplest and easiest to conduct. Still, their accuracy is not very high, especially since a small amount of plated lithium cannot be detected, and the accuracy of detection is seriously affected by the accuracy of voltage measurement. And these common methods are not applicable when charging at high charging C rates, due to it likely being challenging to obtain helpful information about lithium plating from the detection results. It is well known that lithium plating can be divided into reversible and irreversible parts. These detection methods based on voltage variation can only detect reversible lithium plating. Still, if assisted by specific algorithms, these methods can guide whether irreversible lithium plating occurs during charging and discharging,[78] which is vital for analyzing the aging of batteries. Additionally, these methods relying on voltage plateau detection post relaxation or discharging are limited in pinpointing lithium plating during charging. If lithium plating has already occurred in a battery during charging, these methods cannot play a warning role very well, so it is not possible to stop charging in order to prevent lithium plating, which is detrimental to online detection. Each method is described in detail in the following sections.

3.1.1 Voltage plateau analysis. The voltage platform method is the most feasible method for online detection of lithium plating in the battery management system (BMS), which does not require special and expensive equipment, and lithium plating can be monitored in real time. Therefore, in industrial production, monitoring the platform voltage is a practical way to determine whether lithium plating occurs during charging.

The voltage plateau refers to a section of the battery's voltage change that remains relatively flat during the charging and discharging process. In lithium-ion batteries, the voltage plateau is typically associated with the equilibrium state of electrochemical reactions occurring within the battery. During charging, lithium precipitates on the surface of graphite, which strips off during the converse discharging process. Both processes are phase transitions, where the chemical potentials of the two phases are equal at equilibrium, resulting in minimal voltage changes and the emergence of a voltage plateau. By analyzing the corresponding voltage plateaus during charging and discharging, insights can be gained into the lithium plating conditions. It is noteworthy that the insertion of lithium ions into graphite also results in three voltage plateaus, corresponding to the formation of LiC_{24}, LiC_{12}, and LiC_6, respectively.[1] These plateaus exhibit higher voltages compared to the lithium plating plateau, typically above 0 V *vs.* Li^+/Li. When distinguishing whether lithium plating occurs, it is important to differentiate between the lithium intercalation plateaus and the lithium plating plateau.

Regarding the voltage plateau during stripping, Smart *et al.* first applied a low-temperature (−40 °C) discharge voltage plateau as a lithium plating detection tool, as shown in Fig. 3a.[114] They proposed that the plateau length can be used as an indicator for assessing the amount of lithium metal and that the potential of lithium intercalation was inferred as a function of the lithium content. Then Petzl *et al.* studied the discharge curve of commercial cylindrical LIBs at −20 °C. A stripping platform was observed at 70–90% SOC in Fig. 3b, and a uniform silver-white lithium coating was observed on the graphite electrode after the batteries were dismantled, verifying the reliability of the voltage platform representing lithium plating.[115] Next, Yang *et al.* showed that the duration of the voltage plateau period depends on the rate of lithium stripping and that the rate capability of lithium stripping strongly influences the rate capability of lithium embedding into graphite.[117] Then, the voltage profile is very sensitive to lithium plating conditions. Even when the same amount of lithium metal is plated, parameters such as exchange current, insertion density, solid-state diffusivity of graphite, and temperature can significantly affect the voltage profile. Remarkably, regarding the voltage plateau during stripping, Mei *et al.* systematically illustrated the variation of lithium plating voltage with cycles in a Li‖graphite cell, providing cell voltage profiles for four typical cycles during lithiation (Fig. 3c).[116] In the first stage, there is no voltage plateau, but the voltage has been dropping and the potential has been below 0 V, which corresponds to the nucleation process of lithium on graphite. But the voltage cannot drop indefinitely, and a plateau appears, which corresponds to the process of more lithium growth, that is, the second stage. After that, with the increase of the cycle, entering the third stage, there is already a large amount of lithium plated on the surface of the graphite, which is the cell can be regarded as a symmetric cell, so there will be double plateaus. The first plateau is produced by lithium plating, while the second plateau is caused by the stripping of lithium from the Li anode. In the fourth stage, at the last circle of the cycle, during the first plateau period, the cell has been short-circuited due to a large number of lithium dendrites, so there is no "double plateau" feature. While the plateau voltage method can provide a valuable indication of the occurrence of lithium plating, only the reversible portion of the lithium plating can be monitored, and the feature can only be detected when a significant amount of lithium plating occurs.[118]

3.1.2 Relaxation voltage platform analysis. In addition to the voltage plateau during discharging, the voltage plateau during relaxation (rest time after charging) has also been recognized as a simple and effective tool for detecting lithium plating and is widely used in the automotive field. The first attempt to monitor the unique voltage plateau during relaxation after fast charging was made by Uhlmann *et al.*[95] They claimed that the voltage plateau during relaxation instead of discharge, where no net current passes through the open circuit, is more visible and more accessible to analyze. Also, in contrast to

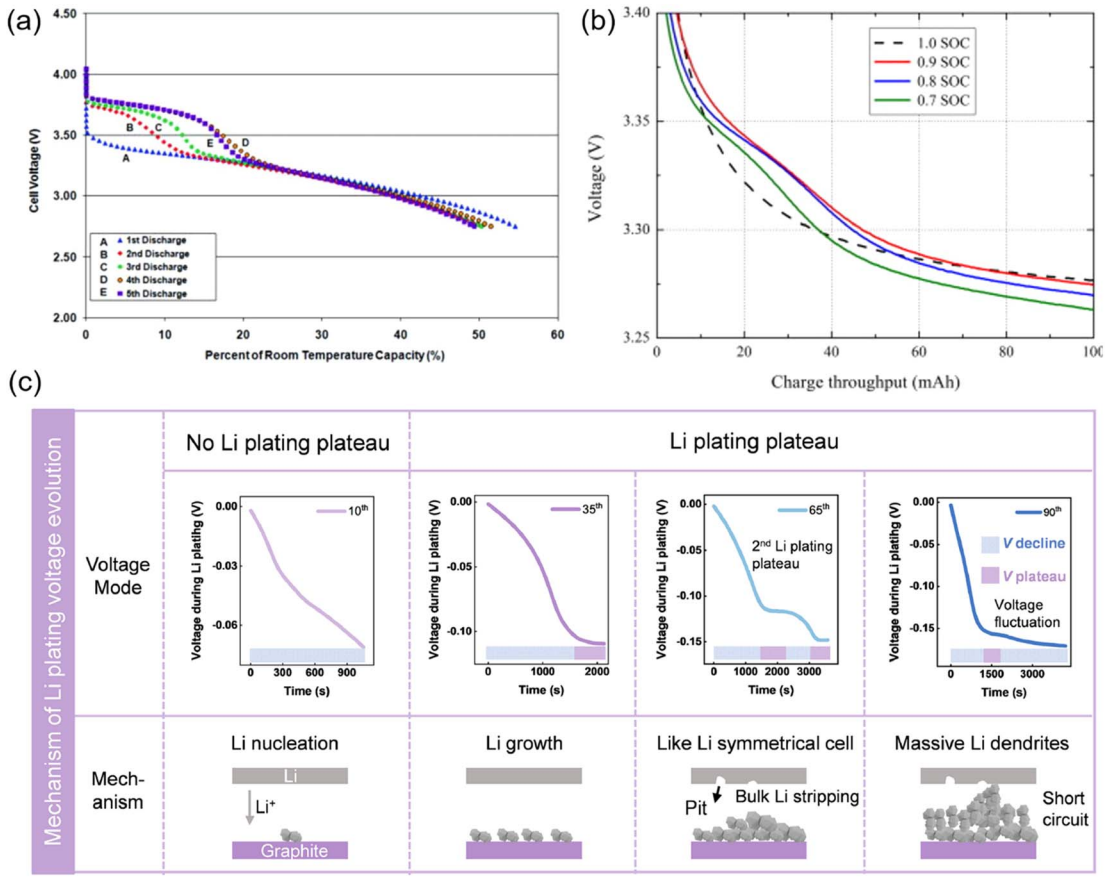

Fig. 3 (a) Discharge curves of a lithium-ion cell at C/20 at −40 °C. Reproduced with permission.[114] Copyright 2011, ECS. (b) Voltage profiles of discharge steps after charging to different SOC levels at −20 °C with 1 C charge current. Reproduced with permission.[115] Copyright 2013, Elsevier. (c) Voltage curves for four typical cycles during the lithium plating process. Reproduced with permission.[116] Copyright 2024, Elsevier.

stripping discharges, voltage relaxation preserves the characteristics of mixed potentials without superimposing any further overpotentials. Then, Fear *et al.* pointed out that the plateau in the relaxation profile indicated re-intercalation of the plated lithium and suggested that significant reversible plating occurs only after a minimum voltage is reached, as shown in Fig. 4a and b.[118] And the absence of a plateau at 20% and 40% SOC suggests that no significant amount of reversible plated lithium was re-inserted during the subsequent resting phase. So similar to the platform voltage method, the absence of re-inserted platforms does not necessarily indicate the absence of lithium plating, and in the case of small amounts of lithium, platforms may not be observed.[117,121] In addition, the relaxation method is not considered to be applicable to the actual operating conditions of electric vehicles, as it requires a rather long relaxation time, which is rarely seen in practice.[41]

A portion of the lithium plated on the graphite surface would be re-embedded into the graphite during the relaxation process, which leads to the typical "double plateau" OCV feature.[45] This plateau is a hybrid potential generated by the interaction of lithium embedding and the dissolution of deposited lithium metal on the anode surface.[46] However, because the voltage change during the relaxation phase is very small, this plateau is sometimes not clear. In order to observe the platform more clearly, the method of differentiating the time of the voltage can be used, which is called the voltage relaxation profile (VRP). S. Schindler *et al.* investigated $LiFePO_4$||graphite cells at different SOCs at −15 °C.[46] In Fig. 4c, a clear localized minimum is seen in the curve for the ΔSOC range of 20–40%. They attribute these changes in the slope to the depletion of the characteristic mixing potentials, thus defining these features as clear indicators of the lithium plating during the previous charging step. In contrast, at ΔSOC = 10%, it is considered that too little charge is transferred, that a critical minimum amount of deposited lithium is not reached during the charging step, and that there are no local minima to characterize. It is possible to quantify how much lithium is deposited by the time at which a localized minimum occurs, with the dV/dt peak indicating the end of lithium stripping. The dV/dt curves were further investigated by Yang *et al.*,[117] and it was shown that the peak in Fig. 4d corresponds to the point at which the amount of lithium metal remaining in the anode is below a certain critical value. In addition, since the curve is essentially converted from a voltage signal, the sensitivity of dV/dt will be limited mainly by the voltage measurement.[46] So this method also has problems of not being able to detect a small amount of lithium plating and

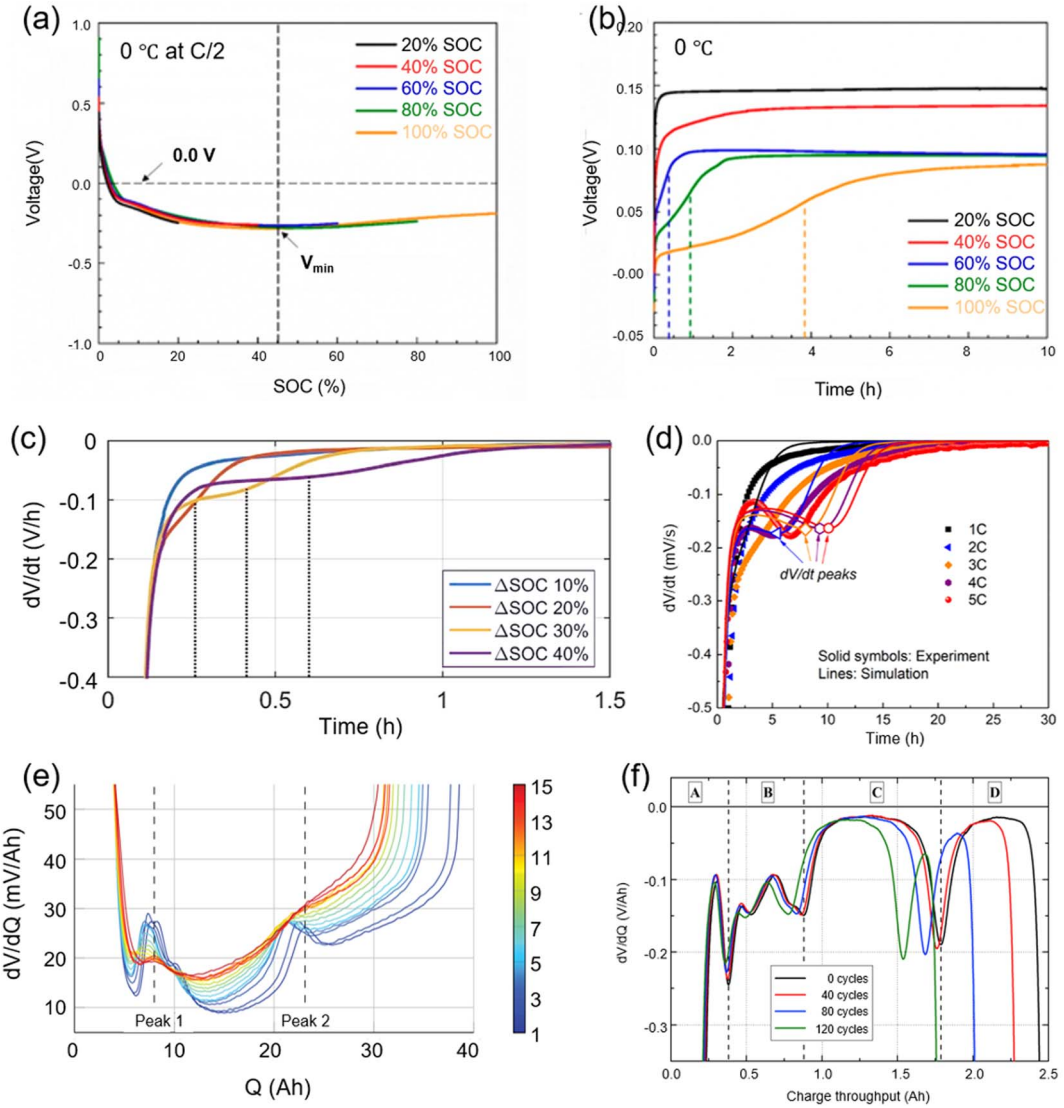

Fig. 4 (a) Relationship between voltage and SOC. (b) Relaxation voltage curves of the cell process at 0 °C and C/2 after charging. Reproduced with permission.[118] Copyright 2020, American Chemical Society. (c and d) Differential voltage over time (dV/dt) in the relaxation process after charging. Reproduced with permission.[46,117] Copyright 2015, Elsevier, Copyright 2018, Elsevier. (e) DV evolution *versus* residual charge Q of a discharged cell. Reproduced with permission.[119] Copyright 2020, Elsevier. (f) Four regions of the DV. Reproduced with permission.[120] Copyright 2014, Elsevier.

a long detection time. In addition, there are also fewer studies of the dV/dt method, and experimental studies are either limited to low temperatures (≤0 °C) or charging to a high graphite SOC.[45]

3.1.3 Differential voltage (DV) and incremental capacity (IC). As with the relaxation process, this voltage plateau is not easy to clearly observe, so two methods are proposed, DV and IC, to convert the plateau into a more easily recognizable differential voltage peak and to identify the lithium plating process. DV and IC are inversely related, which can *in situ* detect lithium plating quantitatively.[78] The basic principle of both is also based on the fact that if lithium plating occurs during charging, lithium stripping will occur during discharging, which is reflected in the time–voltage diagram by the appearance of a high-voltage plateau and appears before the first normal de-embedding plateau of the graphite anode.115 The DV method calculates the derivative of the voltage V with respect to the capacity Q during the discharging process,[119–122] whereas the IC is the opposite, the derivative of the capacity Q with respect to the voltage V.[113,123–127] The main difference between these two derivatives is that the peaks in the dV/dQ curves represent phase transitions, while those in the dQ/dV curves represent phase equilibria.[128] Another difference is that dQ is always non-zero for DC analysis relative to IC. The derivative of voltage to capacity, dV/dQ, is well suited for the graphical analysis of cell data.

The derivative dV/dQ signifies the variation of voltage per unit capacity, embodying the responsiveness of voltage to changes in capacity during the reverse charging and discharging cycles.[78] Typically, the progression of battery voltage with

respect to capacity is smooth, and is attributed to the relatively consistent and continuous electrochemical reactions occurring within. Nevertheless, in instances where a phase transition or structural alteration takes place, the voltage variation may intensify or exhibit abrupt changes, heightening its sensitivity and culminating in the emergence of a peak in the voltage–capacity curve.[119]

There are several reasons for the abrupt change in the curve: (1) phase transition barrier. Lithium plating can be viewed as a phase transition, which is a complex phenomenon involving thermodynamic and kinetic processes. In this process, the system needs to overcome certain energy barriers such as the lithium nucleation and growth barriers on the surface of graphite, which causes a sharp change in the voltage signal near the phase transition point. (2) inhomogeneous electrochemical reaction: when lithium plating occurs, the electrochemical reaction cannot be as smooth as usual. The formation of lithium plating on graphite exhibits both temporal and spatial non-uniformity, requiring an additional voltage to overcome this non-uniformity. Consequently, the non-uniformity during the phase transition contributes partially to the generation of peaks in the curve. (3) change of internal resistance: the internal resistance of a battery is one of the critical factors influencing its voltage variation. After the formation of lithium plating, the internal resistance will change, subsequently affecting the voltage performance during charging and discharging. This variation in internal resistance further exacerbates the non-smoothness of the battery voltage as it changes with capacity. (4) obstruction of ion and electron transport: during the lithium plating process, the SEI layer on the surface of graphite grows thicker, hindering the transport of lithium ions to a certain extent. Additionally, lithium plating alters the charge transfer impedance of the graphite anode, both of which impact the electrochemical reaction rate, leading to sharp changes in the battery voltage.

The peaks on the DV curve specifically reflect the peaks indicating the phase transition between the different graphite intercalation phases,[120] with the change in the height of the peaks (ΔPeak1, ΔPeak2) indicating the degree of homogeneity of the lithium distribution in the cell,[119] and the peak shift and the corresponding change in capacity are used to analyze the contribution of the different aging mechanisms, including lithium plating, as shown in Fig. 4e. The first additional peak at the beginning of the DV curve indicates the presence of lithium plating prior to discharging, and the amount of lithium plating is related to the corresponding capacity of the additional peak. In DV research, Petzl *et al.*[120] achieved further analysis of the aging behavior by dividing the DV curve into four regions (Fig. 4f). The high-voltage region D exhibits the greatest capacity loss. Regions B and C show much smaller decreases, while region A is hardly affected by the low-temperature cycle. This behavior, *i.e.*, the significant capacity loss in region D, is characteristic of cyclable lithium loss. After that, Lewerenz *et al.* used differential voltage in $LiFePO_4$‖graphite to analyze cells with different temperatures, charging rates, and SOCs.[122] Based on this, the relationship between cyclic aging and lithium distribution uniformity of the batteries was systematically investigated. The different uniform distribution of active lithium during the aging process will lead to different phenomena. Fairly low uniformity results in reduced capacity because the cut-off voltage is reached in advance and may cause lithium plating during charging. Then, Campbell *et al.* pointed out that the differential voltage signature, which is a complex composite of two complex individual electrode potentials, can also be used in detection and quantification in commercial batteries using voltage platform techniques.[121]

In IC, dQ/dV represents the change in capacity per unit voltage change, reflecting the fluctuation of battery capacity at a specific voltage. As shown in Fig. 5, within a certain voltage range, dQ/dV exhibits a low slope without the presence of peaks, which corresponds to a process where the voltage changes significantly while the capacity changes minimally. The emergence of peaks indicates that the battery is able to release or absorb a large amount of energy at a relatively constant voltage, manifesting as a voltage plateau in the voltage curve. The appearance of voltage plateaus typically corresponds to the steady-state phase of specific electrochemical reactions occurring within the battery, where these reactions proceed at a relatively constant rate. During lithium plating, a plating plateau appears in the voltage curve, resulting in an additional peak appearing in the dQ/dV curve as well.

Each peak in the IC curve has a unique shape, intensity, and location, and it exhibits the electrochemical process occurring in the cell.[124] And in the IC, the peak characteristics produced by reversible lithium plating and irreversible lithium plating are different. For reversible lithium plating, a new peak (peak 0) will appear when high voltage is present in the IC curve; meanwhile, for irreversible lithium plating, not only does peak 0 appear, but also the strength of peak 1 will be reduced (Fig. 5a). In IC, the decrease of peak 1 usually originates from the formation of thick SEI and dead lithium, both caused by lithium plating.[78]

Compared to DV, IC is able to detect lithium plating in different types of batteries, although it may present some difficulties in mapping. Moreover, IC can be used to calculate the stripping voltage of lithium plating, which is more suitable in the severe stage of rapid charging aging. In IC research, Dubarry *et al.* qualitatively identified and analyzed the main causes of capacity degradation, *i.e.*, loss of active material (Fig. 5b), changes in battery chemistry (Fig. 5c), under-discharge and under-charge (Fig. 5d).[123] Then in their another study,[124] it was stated that the polarization effect must first be eliminated so as to better understand the IC behavior of the chemistry in the battery. After eliminating it, the IC peaks broaden at an increasing rate, and additional kinetic effects are still in play, which do not affect each IC peak in the same way. And in the quantitative analysis of IC, Anseán *et al.* combined incremental capacity and peak area analysis to identify features.[127] Combined, they helped to identify and quantify the presence of a new phase transition in the characterization, which emerged from the emergence of reversible lithium plating. IC analysis was also applied to multilayer pouch cells with and without a three-dimensional anode structure. Finally, the evolution pattern of the plated IC peaks during extended fast charging cycles was investigated. It revealed that the decrease in the

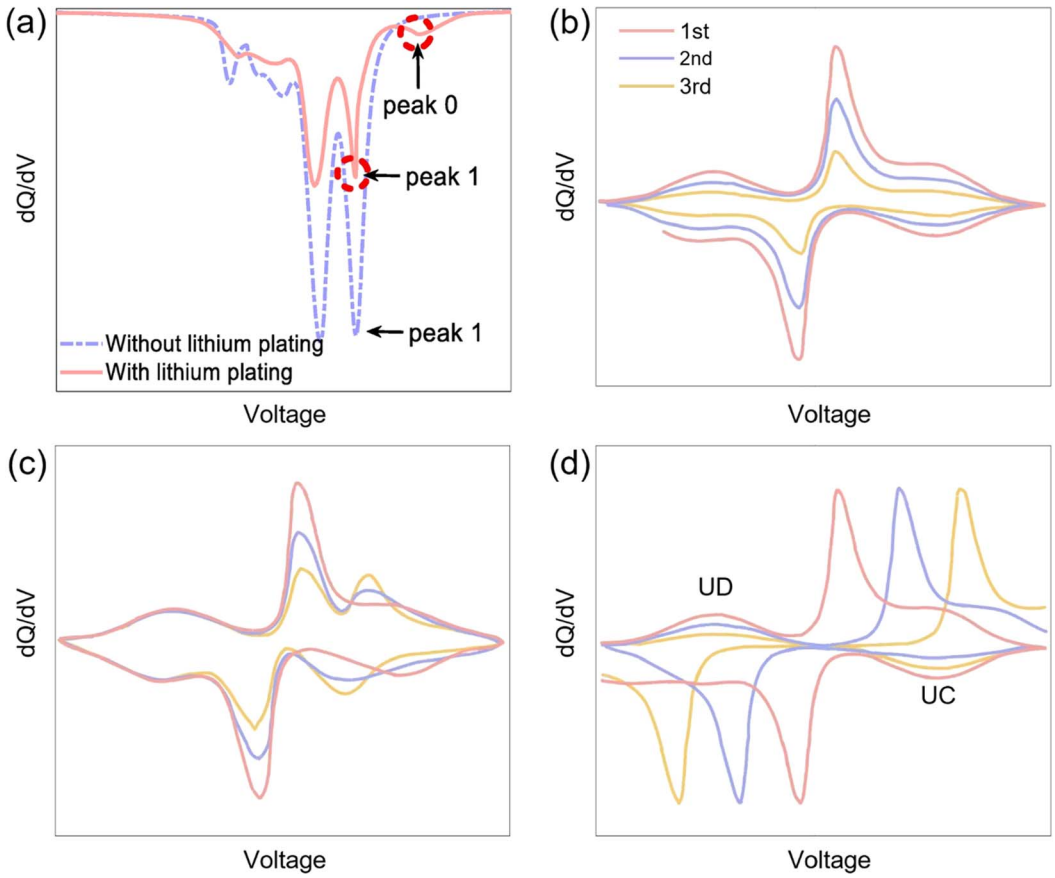

Fig. 5 (a) Detection principle of the IC method (the red dotted circles highlight the occurrence of lithium plating). Reproduced with permission.[78] Copyright 2021, Elsevier. (b–d) Evolution of IC curves, hypothetically in the case of (b) loss of active material, (c) changes in battery chemistry, and (d) under-discharge (UD) and/or under-charge. Reproduced with permission.[123] Copyright 2006, ECS.

amplitude of the plated IC peaks was correlated with an increase in CE, which was attributed to a decrease in the lithium increment of the plated layer during each fast charging cycle and a decrease in the lithium inventory during the extended cycles.

The drawbacks of both methods are also evident, such as the use of both DV and IC needs to be performed at lower current discharges. Interpretation of cell differential curves has been challenging when charging rates are higher than 1C, as some of the peaks in the higher rate differential curves (related to electrode phase changes during interpolation) could not be clearly recognized at higher rates.[113,129] For example, when analyzed using IC, a low-magnification interpolation peak can be observed, but a distinct additional peak appears when discharged at higher than 2C, and the peak size and position of the low-magnification peak is constantly changing, making it difficult to accurately account for the process represented by the peaks if measurements are made at only one discharge rate (without comparisons), which is obviously very detrimental to analyzing the lithium plating process. Likewise, similar to other conventional methods, DV and IC can only detect reversible lithium but not irreversible lithium. Moreover, if one wants to detect lithium plating by DV accurately, the cell must be discharged immediately after charging to avoid the influence of the relaxation process on voltage detection.[78]

3.1.4 Three-electrode. Lithium plating is an internal process within the battery, and visualizing the process usually requires the use of a microscope, which is destructive.[23] However, external features that could be measured by not disassembling batteries can reflect internal reaction processes in batteries,[42,70,130] and measuring the anode potential with a reference electrode is an indirect measurement. In a full cell, the voltage is the difference between the potentials of the anode and the cathode. If there are only two electrodes in the cell, there is no way to decouple the potential of the single electrode. With the inclusion of a reference electrode, it becomes possible to accurately obtain the potential at the graphite electrode–electrolyte interphase (Fig. 6a). If this obtained potential is below 0 V (*vs.* Li^+/Li), as illustrated in Fig. 6b,[46] it suggests the occurrence of lithium plating.[133]

Conventional lithium reference electrodes are relatively large in size, which can change the overall structure of the cell and thus affect the working environment inside the cell.[60] A large number of studies have been conducted on copper wire reference electrodes derived from the electrochemical deposition of lithium. Zhou and Notten improved these reference electrodes by electrochemically depositing lithium metal from the cathode

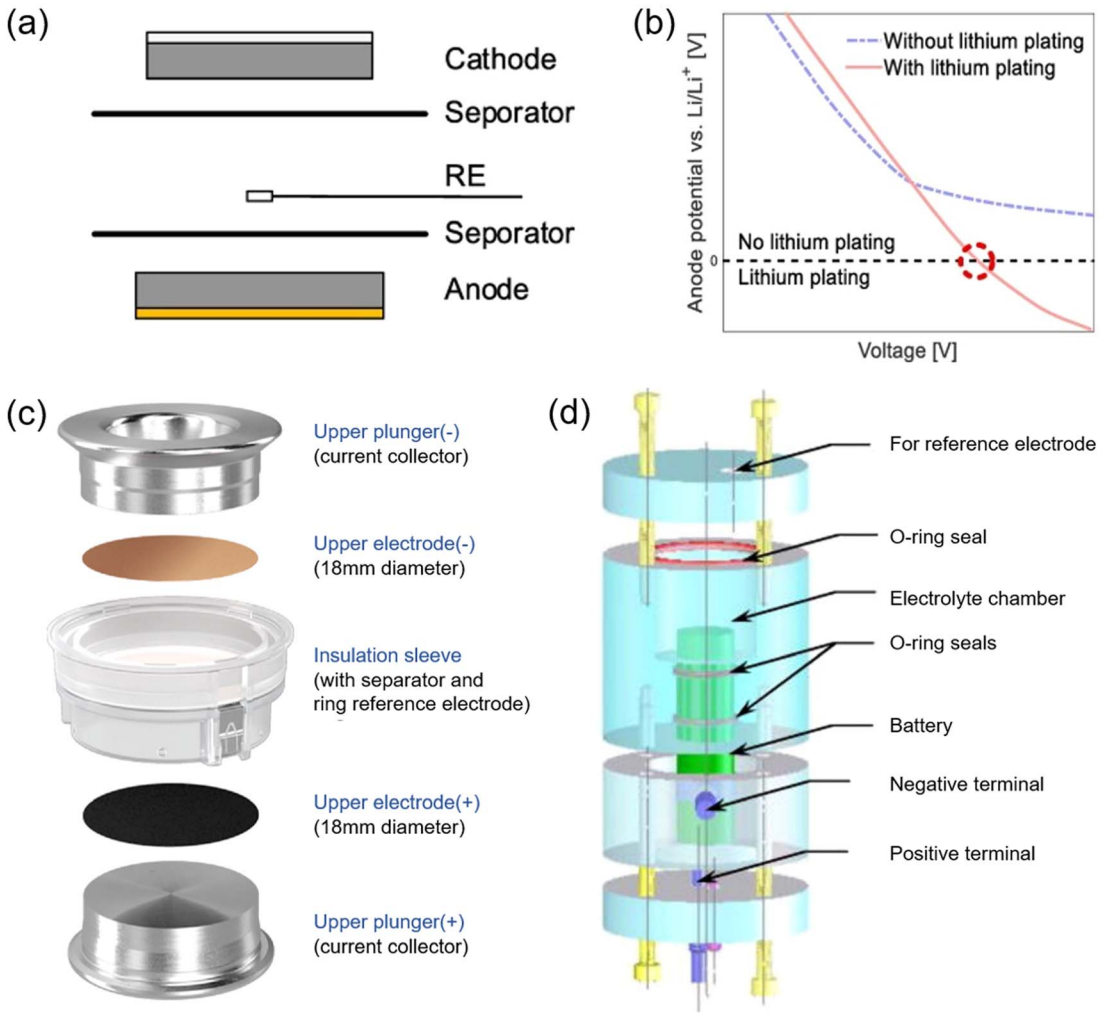

Fig. 6 (a) Schematic diagram of the three-electrode cell. (b) The detection principle of the anode potential measurement (the red circle highlights the occurrence of lithium plating). Reproduced with permission.[78] Copyright 2021, Elsevier. (c) Traditional structure and components of a cell holder for a three-electrode cell with a lithium-metal reference electrode. Reproduced under terms of the CC-BY license.[136] Copyright 2023, The Authors, published by Elsevier. (d) A cylindrical three-electrode structure. Reproduced with permission.[132] Copyright 2009, ECS.

and anode onto copper wires to form micro-reference electrodes, which can effectively solve the defects of the large size of the reference electrodes and can be adjusted by regulating the current density and thickness of the lithium layer of the electrochemical deposition to improve the performance of reference electrodes.[134] In addition, there are some other types of reference electrodes, such as Li–Au alloy,[135] $Li_4Ti_5O_{12}$,[136] and lithium-tin reference electrodes.[137]

The position of the reference electrode directly determines the potential error of the reference electrode, so the accuracy of lithium plating detection can be optimized by improving the position of the reference electrode. The reference electrode is typically located between the anode and cathode to minimize the ohmic voltage drop and accurately measure its potential.[133] Simulations by Dees *et al.* also showed that the optimal location for the reference electrode in a LIB is between the anode and cathode.[138] The general reference electrode is placed between the anode and cathode, as patented by EL-Cell GmbH (Hamburg, Germany) for its so-called PAT-Cell (Fig. 6c). The separator is sandwiched between the two halves of the sleeve, which contain an electrode and a plunger as a fluid collector is pressed against the separator outside the electrode region. Or a reference electrode (usually comprising a lithium metal disk) is placed perpendicular to the anode and cathode outside the active region. The integration of reference electrodes in flexible pack batteries is usually more complicated compared to coin cells. However, the *in situ* three-electrode method developed by Zhang *et al.* allows for the measurement of cathode and anode electrode potentials as well as full-cell voltages during charging/discharging performance testing, as depicted in Fig. 6d.[132] This *in situ* three-electrode method does not change the electrode–electrolyte or the electrode microstructure. After that, Drees *et al.* optimized a method of reference electrode placement by placing the reference electrode near the anode protrusion and cathode edge of a pouch cell.[131] This location does not require additional mounting space, and the reference electrode is also outside of the active electrode region, which does not affect the cell's performance. By placing the reference electrode in the

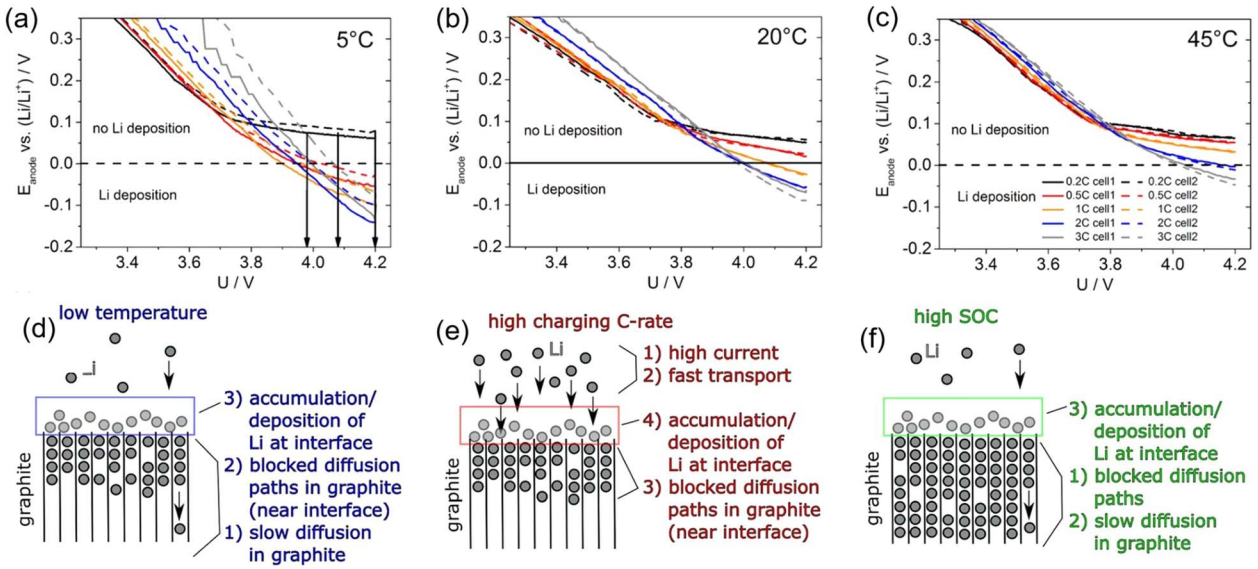

Fig. 7 (a–c) Anode potentials *vs.* (Li^+/Li) measured in reconstructed three-electrode full cells at ambient temperatures of (a) 5 °C, (b) 20 °C, and (c) 45 °C. (d–f) Model of the influencing operational parameters on the deposition of lithium on graphite anodes: (d) low temperatures, (e) high charging C rates, and (f) high SOC. The numeration corresponds to the argumentation order of the respective explanations. The boxed areas correspond to the solid|liquid interface, where the Li deposition happens. Reproduced under terms of the CC-BY license.[133] Copyright 2016, The Authors, published by ECS.

above methods, the anode potential can be detected more accurately, so as to obtain more accurate lithium plating information. For example, T. Waldmann *et al.* quantitatively and systematically investigated the relationship between the negative anode potential and lithium plating during the charging process of LIBs by using a reconfigured three-electrode pouch cell, mainly measuring the anode voltage at different temperatures and charging C rates, and it is not difficult to draw the conclusion that lithium plating tends to occur at low temperatures and high charging C rate, as shown in Fig. 7a–c.[133] Similar conclusions were also reached by three-electrode experiments by Zhang *et al.*[139] And the reasons for low temperature, high charging C rate, and high SOC lithium plating are discussed in Fig. 7d–f, which is mainly ascribed to the blocked diffusion path of lithium inside the graphite layer, and lithium ions cannot be quickly inserted into the graphite. A large amount of lithium is deposited on the SEI, resulting in lithium plating.

3.2 High-precision measurement methods

Even small amounts of lithium plating during battery cycling can shorten battery life and affect safety performance, so higher sensitivity for detecting lithium plating is needed. Impedance-based methods and high-precision coulombic efficiencies (CEs) are very sensitive to lithium plating and can be tested at a high charging/discharging C rate. However, these methods have the obvious disadvantage of not being able to fulfill the need for real-time monitoring, which is detrimental for applications in BMS. In addition, these methods require additional testing equipment. They are explained in the following sections.

3.2.1 High-precision coulombic efficiency (CE). Theoretically, reversible lithium plating does not cause a loss of capacity because it is simply another way of accommodating capacity.[45] In contrast, the irreversible lithium plating may become electrically isolated from the graphite electrode during stripping. So irreversible plating is the main cause of capacity loss during low temperature and high current charging. But the growth of the SEI isn't taken into account. The plated lithium is capable of growing through the SEI layer and engaging in a reaction with the electrolyte, ultimately leading to a decrease in overall capacity. Consequently, the capacity degradation stemming from lithium plating encompasses the stripping of irreversible plated lithium as well as the lithium consumed by the growth of the SEI layer.

Also, for small amounts of lithium plating, since the reversibility of the lithium plating/stripping process is relatively low compared to lithium intercalation/de-intercalation in graphite,[41] only a reversible part of a small amount of lithium plating can be detected by observing voltage changes, so a trace amount of lithium cannot form a voltage platform to indicate the occurrence of lithium plating. So it is unwise to use the detection of voltage changes to determine whether lithium plating has occurred or not, and therefore non-destructive testing can be achieved by conducting high-precision measurements of the CE. The coulombic efficiency, defined as the ratio of discharge and charge in a cycle, serves as an indicator of capacity loss. This reduction in CE can effectively detect the occurrence of lithium plating.

Burns *et al.* reported small changes in CE during low-temperature charging using a high-precision charger to analyze lithium plating, and they first pointed out the relationship between cycle multiplicity and CE at different temperatures, as shown in Fig. 8.[140] As the charging rate is gradually increased, the CE should change almost exactly to 1.0

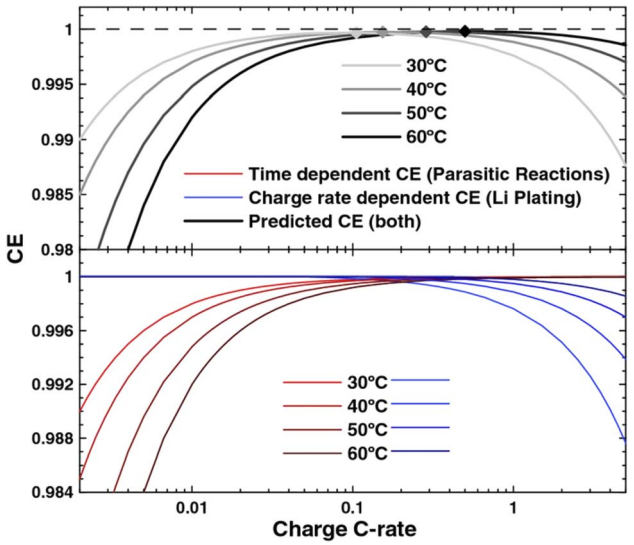

Fig. 8 Schematic of CE *versus* charging C rate with both the time-dependent and charging C rate-dependent resolved curves (bottom) and the resulting CE *versus* rate curve (top) at different temperatures. Reproduced under terms of the CC-BY license.[140] Copyright 2015, The Authors, published by ECS.

because the time for parasitic reactions and degradation of the cells to occur is shortest in each cycle. Continuing to increase the cycling charging C rate after that, lithium plating will occur and cause the CE to deviate from 1.0. Later, by disassembling the battery and observing the electrodes, it was confirmed that the CE began to decline as an indicator of lithium plating.

CE is more effective than other methods in detecting irreversible lithium plating and can detect lithium plating in the middle and late stages of the entire cycle. Using a high-precision charger can significantly improve detection accuracy. However, there are several limitations to consider. Over long-term cycling, batteries will experience side reactions beyond lithium plating, such as increased resistance due to compromised electrical contact with the active material or obstructed electrode pores. These factors greatly complicate the analysis of lithium plating. Additionally, the scarcity of high-precision voltage measurement equipment poses a challenge. Commercial batteries often exhibit sufficiently high CE levels that standard equipment fails to identify minor CE fluctuations. To implement high-precision efficiency assessment techniques, substantial investment in sophisticated equipment is necessary.

3.2.2 Impedance based approaches

3.2.2.1 Electrochemical impedance spectroscopy (EIS). There are several major components that can cause impedance changes during charging and discharging of LIBs, migration of lithium ions through the SEI layer, charge transfer impedance at the interface, and diffusion impedance of lithium ions.[45] The core of EIS is to distinguish different rates of electrochemical reaction processes by impedance changes at different frequencies. Therefore, by using EIS, these processes with varying constants of time can be effectively identified. Moreover, EIS only applies a small amplitude sinusoidal signal to the system, and the electrodes are alternately subjected to cathodic and anodic processes during the test, which does not cause an accumulation of polarization phenomena.

The Nyquist plot is usually presented after an EIS test on LIBs. It consists of two semi-circular arcs and a straight line with a slope close to 45°, as shown in Fig. 9a. From left to right the frequency of the process is represented as it decreases in order, with the leftmost point of intersection of the first semi-circular arc with the horizontal axis representing the magnitude of the ohmic impedance. The first semi-circular arc represents the impedance of the lithium-ion through the SEI layer, the second semi-circular arc is the charge transfer impedance, and the rightmost diagonal line is the diffusion impedance. The corresponding equivalent circuit is shown in Fig. 9b.

Plating was detected by impedance spectroscopy during voltage relaxation by S. Schindler *et al.*[46] As shown in Fig. 9c, the main arc at $f = 5$ Hz corresponds to the charge transfer impedance of graphite, and it is not difficult to see that the impedance gradually increases with the increase of rest time. This indicates that lithium is embedded into the graphite causing the impedance to rise. In this way, it is indirectly proved that the decline of impedance is the key sign of lithium plating during the charging process. Similar results were obtained by Pan *et al.*[141] Next, Brown *et al.* applied the operational impedance analysis to a two-electrode full cell (Fig. 10a–d).[142] If there were no plating, the graphite SEI response would be unchanged, and the whole cell would reflect only a monotonic decrease in the $LiNi_{0.5}Co_{0.2}Mn_{0.3}O_2$ high-frequency process, as shown in Fig. 10d. However, if plating does occur on some of the SOCs, the increase in graphite SEI impedance will offset the decrease in $LiNi_{0.5}Co_{0.2}Mn_{0.3}O_2$ impedance. In fact, Fig. 10c clearly shows this behavior. In summary, the effect of lithium plating on the impedance of the graphite anode is mainly manifested as the increase of interface impedance and the decrease of charge transfer impedance of the SEI. After lithium plating, the SEI interface layer becomes thicker, resulting in slower lithium ion transport, which in turn leads to increased interface impedance. And the reason for the reduced charge transfer impedance may be that the surface area of the anode is increased after lithium plating, making charge transfer easier.

The advantages of EIS are undeniable; it is a very convenient non-destructive testing technology, and the measurement results are very sensitive to the weak changes in the impedance of the cell, making the accuracy very high. However, in the actual measurement process, the distribution of time constants of the processes inside the cell is likely to deviate from the ideal distribution, resulting in two semi-circular arcs overlapping together, or a process impedance is relatively small, resulting in the small semi-circular arc difficult to be recognized. These faults are very unfavorable for EIS analysis.

3.2.2.2 Dynamic electrochemical impedance spectroscopy (DEIS). The basic principle of DEIS is to superimpose a sinusoidal current with a small amplitude on the charging current during the test, and obtain the battery EIS impedance according to the changing sinusoidal current without interrupting the charging and discharging. In contrast to conventional EIS

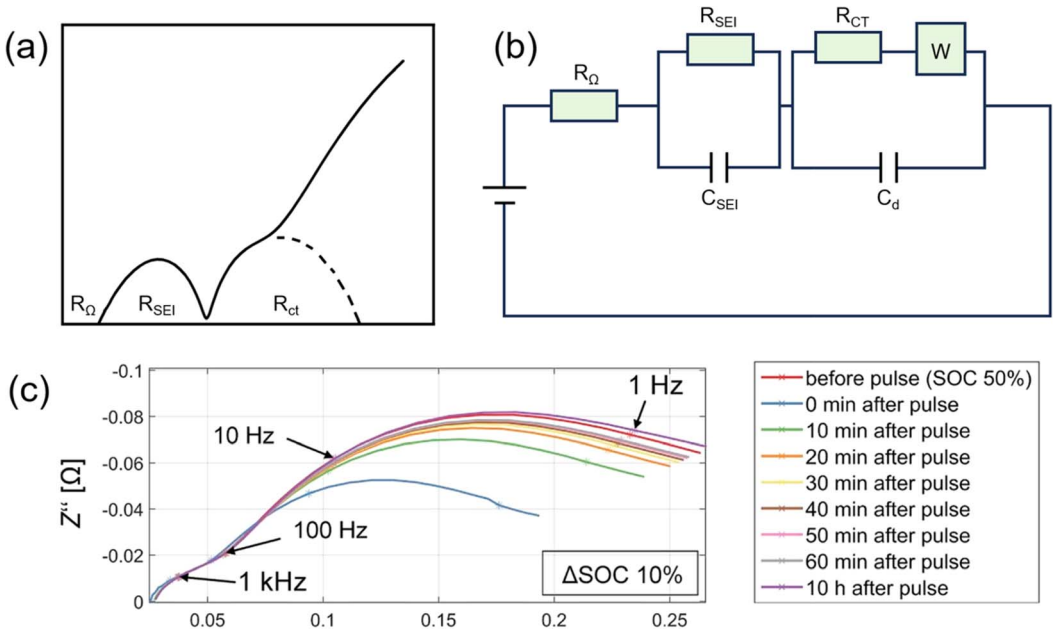

Fig. 9 (a) A typical Nyquist plot. (b) An equivalent circuit diagram. (c) Evolution of impedance spectra for experiments at $T = -15$ °C, ΔSOC = 10%, Ich = 2 Cnom. Reproduced with permission.[46] Copyright 2015, Elsevier.

analysis, with DEIS it is not only possible to detect lithium plating in real-time without cutting off the voltage but also to continue charging after the test has been performed. At the same time, compared with EIS, DEIS is significantly simpler in data processing and can more clearly and intuitively show the impedance changes during lithium plating. Traditional EIS also has the advantage that the measurement frequency range can be set according to the need, and the test can be conducted at a very wide frequency to obtain the impedance of multiple processes in the LIBs, such as ohmic impedance, SEI interfacial layer impedance, charge transfer impedance, diffusion impedance, *etc.* In contrast, the DEIS technique can only set the alternating current frequency to a specific value during the test, usually the frequency corresponding to the impedance change process during charging and discharging, to better analyze the change of impedance during charging.

DEIS was first applied by Koseoglou *et al.* to study the impedance variation during lithium plating.[143] They pointed to a sudden drop in the battery's interface impedance as a sign that lithium plating had begun. The DEIS technique was also

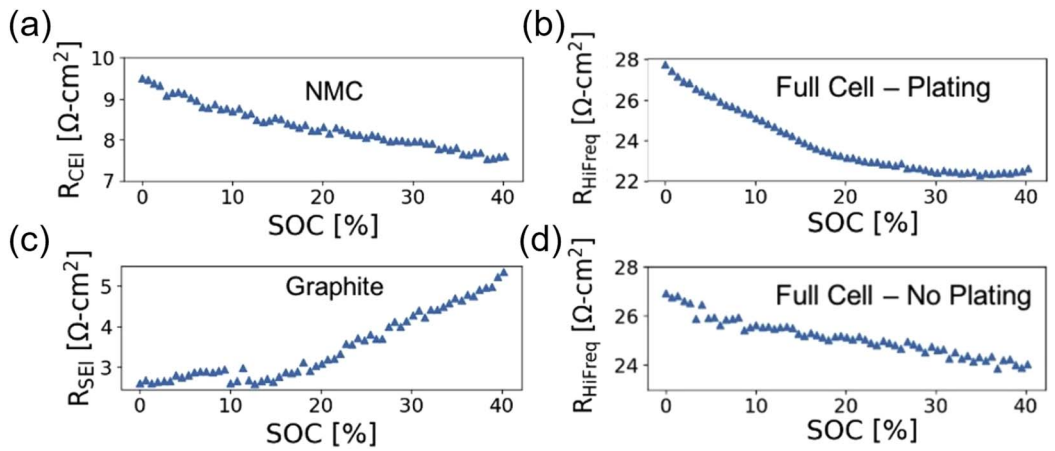

Fig. 10 Comparison of graphite and $LiNi_{0.5}Co_{0.2}Mn_{0.3}O_2$ high-frequency impedance during fast charging to full cell impedance. (a) The high-frequency resistance related to CEI and/or interparticle resistance on $LiNi_{0.5}Co_{0.2}Mn_{0.3}O_2$ during a 4C charging. (b) This signal occurs in the same frequency regime (~10^4 Hz) as graphite SEI resistance during a 4C charging. (c) The sum of these two impedance processes—"R_{HiFreq}"—is measured in a $LiNi_{0.5}Co_{0.2}Mn_{0.3}O_2$||graphite two-electrode cell during a 4C charging where plating occurs. (d) The same impedance frequency region as (c) but for a cell wherein impedance does not indicate lithium plating. Reproduced under terms of the CC-BY license.[142] Copyright 2021, The Authors, published by Elsevier.

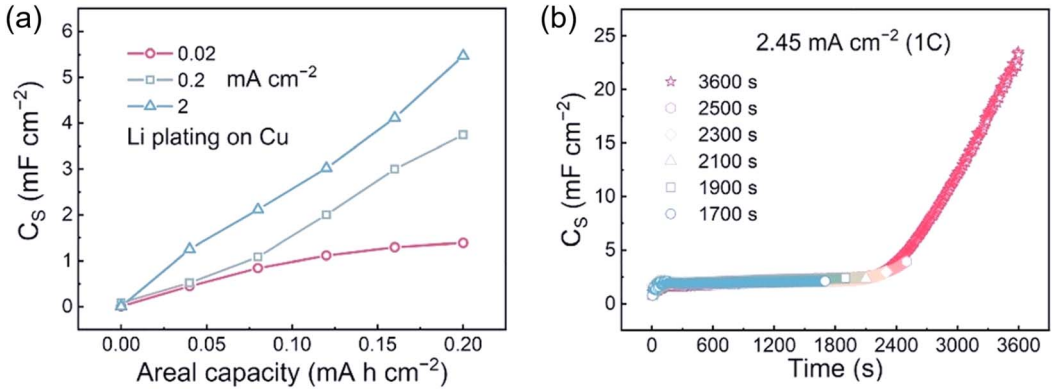

Fig. 11 Validation of DEIS in Li plating determination. (a) Variation of C_S values (C_S reflects the value of the EDL capacitance) on Cu at 0.02, 0.2, and 2.0 mA cm^{-2}. (b) DEIS tests on graphite at 2.45 mA cm^{-2} (1.0C). Reproduced with permission.[144] Copyright 2022, Wiley-VCH.

used to reveal the relationship between the graphite anode's double-decker capacitance and the electrochemically active surface area during lithium-ion intercalation and lithium plating processes.[144] By relating the electrochemically active surface area to the anode's double electric layer (EDL) capacitance, an initial lithium plating mechanism is proposed. Thus, the EDL capacitance of the graphite anode surface is defined and directly correlated with the impedance results detected by the DEIS. The single-frequency DEIS test allows real-time monitoring of the capacitance changes of graphite anodes under dynamic conditions. In Li||Cu, Li||graphite verified that the rise in capacitance indicates the onset of lithium plating (Fig. 11). Impedance and capacitance values are inversely proportional to each other, so the increase in capacitance means a decrease in the charge transfer impedance of the graphite anode. This shows that in DEIS testing, a sharp decline in impedance is still a key indicator of lithium plating.

3.2.2.3 Distribution of relaxation times (DRT). The relaxation time is the time required for a system variable to change from a transient state to a steady state.[41] In battery systems, the relaxation time corresponds to the characteristic time constants of different physical and chemical processes. Real battery systems have complex microstructures with specific time distributions for each process. Correspondingly, by extracting the distribution of relaxation times from EIS data, different electrochemical processes can be identified and understood from different peaks. There has been a lot of work explaining the principle of DRT and the derivation of the equations in detail,[145–147] and this article will not elaborate on it.

For coin cells, DRT results are generally evaluated in the frequency range of 100 k–0.1 Hz. In order to better trace the peak correspondence process in the DRT results, Chen *et al.* investigated the impedance spectrum and DRT results for half-cells.[148] As shown in Fig. 12a, for the anode half-cell, a large impedance is exhibited at 0% SOC. Once lithiation starts, the impedance changes abruptly and exhibits a slight change during the subsequent discharging process. This phenomenon may be due to the change in the physicochemical properties of graphite after lithium embedding occurs. There are four peaks in the DRT (Fig. 12b). N1 is thought to be attributed to contact impedance because the corresponding frequency is the highest. N2, which lies in a similar frequency range, may come from the lithium counter electrode and the SEI. It is hypothesized that N3 and N4 may be related to the charge transfer process in graphite. The nature of the full cell is a superposition of the cathodic and anodic parts, so the contribution of the intrinsic reaction process of the two electrodes can be distinguished by comparing the DRTs of the full and half cells. In the following, by determining the attribution of the peaks, the DRT information can be used to estimate whether lithium plating is

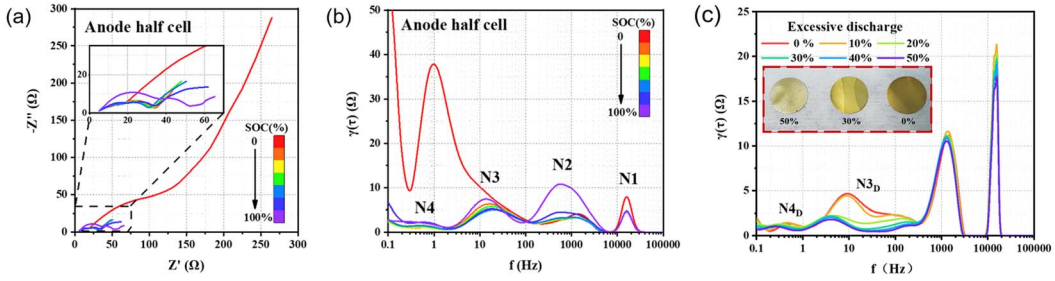

Fig. 12 (a) EIS and (b) DRT results of the anode half cell and (c) DRT results of the graphite half cell over-discharge with excessive capacity from 0 to 50% and a digital photograph of the graphite anode with different amounts of lithium plating. Reproduced with permission.[148] Copyright 2021, Elsevier.

occurring and to analyze the internal changes in the lithium-plated cell.

Lithium plating is a process that occurs at the anode, and analysis of the DRT of an anode half-cell reveals that increasing the amount of lithium plating causes $N3_D$ to mutate and move to a lower frequency of about 4 Hz, with a significant decrease in intensity. This is a clear sign of lithium plating, as shown in Fig. 12c. The transformation of the EIS impedance spectrum using DRT analysis has the apparent advantage of better visualization of the information contained in the EIS, and the transformation of the half arcs into the form of peaks allows for a more explicit determination of lithium plating. In the EIS analysis, the relative size of the impedance under different SOCs may vary greatly, resulting in multiple SOCs being presented in a single graph when analyzed, so the smaller impedance part cannot be clearly presented. At the same time, there are also LIBs in different processes with very similar time constants leading to the superposition of semi-circular arcs making them difficult to distinguish, and the use of DRT analysis can obviously solve these defects, so the analysis results are more clear. At the same time, according to the change of the peak value, the amount of lithium plating can be quantitatively judged, as well as the length of time for which the lithium plating occurs. For example, Brown *et al.* used a small current to charge the battery, and lithium plating did not occur before the graphite was completely lithiated.[142] When SOC is greater than 100%, lithium plating occurs, the peak value of charge transfer impedance decreases, and the amount of lithium plating is quantitatively analyzed according to the decrease of peak value. It is also shown that this method can be used to quantify the lithium plating under the condition of a high current of 6C.

3.2.2.4 Nonlinear frequency response analysis (NFRA). NFRA is a novel method for the dynamic analysis of LIBs. In contrast to the most commonly used EIS, NFRA is not limited to the linear response of the system, and additional dynamic information about the system can be obtained. Harting *et al.* were the first to apply the NFRA technique to LIBs, correlating the NFR spectra with the impedance spectra on the LIB pouch cell, and showed that, where EIS could not be distinguished, it was possible to isolate and identify the contribution of the solid diffusion in the SEI, the reaction and ion contribution of processes such as transport.[149] The NFRA method can be considered a critical additional dynamic analysis method for dynamic LIB characterization. In a later study,[150] NFRA was used to analyze lithium plating in pouch cells, where the higher harmonic responses, such as the third harmonic, differ when lithium plating occurs. Murbach *et al.* used a pseudo-two-dimensional Doyle–Newman impedance model and simulated the higher harmonic responses of the LIBs.[151] They showed that the second highest harmonic response is sensitive to the charge transfer response in the electrode.

3.3 Other methods

In the recent past, researchers have also developed new electrochemical methods for the detection of lithium plating, and due to a lack of research, the accuracy of these methods as well as the conditions for their use are not yet clear. They are described in the following sections.

3.3.1 Average voltage estimation. This is a method of identifying the start of unwanted lithium deposition based on the average voltage of the battery during charging and discharging, and it is applicable to any battery, where the calculation is done by dividing the energy by the capacity.[152] The two most important factors affecting the average voltage of a LIB under load are the increase in internal resistance and the loss of lithium inventory. Increases in internal resistance and loss of lithium inventory have a linearly additive effect on the average voltage; therefore, tracking the average of the charge voltage and discharge voltage *versus* the cycle counts allows one to determine where rapid changes in lithium inventory begin, thus indicating the onset of unwanted lithium deposition. The change in average voltage attributable to impedance growth will hereinafter be referred to as the resistance voltage (RV), and the change due to loss of lithium inventory is referred to as the shift voltage (SV). The formulae for calculating SV and RV are shown in eqn (5) and (6), respectively. Ideally, an ion battery should have a constant average charge voltage ($V_{av,c}$) and a constant average discharge voltage ($V_{av,d}$) over its lifetime. However, the battery's $V_{av,c}$ increases and $V_{av,d}$ decreases during the actual long cycle, as shown in Fig. 13a, and the SV after performing the zeroing process is referred to as the shift voltage change (SVC). Lithium plating is marked by a shift in the trend of the SVC from decreasing to increasing (Fig. 13b), *i.e.*, the sharp increase in the SVC is due to the rapid loss of lithium inventory, which is attributed to lithium metal deposition.

$$SV = 1/2(V_{av,c} + V_{av,d}) \quad (5)$$

$$RV = 1/2(V_{av,c} - V_{av,d}) \quad (6)$$

Detection of lithium plating using the average voltage method is an extremely simple method that requires only the most common instruments to measure voltage and capacity. However, as a new method, the mechanism and accuracy of the method are not clear. It is only applicable to the detection of lithium plating during cyclic aging, and the applicability to a single cycle is not clear.

3.3.2 IR drop method. An *in situ* analysis method based on transient analysis to detect the onset of lithium plating at room temperature under high magnification operating conditions was recently proposed.[153] The iR drop was dissected to decipher the resistance on the graphite anode by an equivalent circuit method. A three-electrode cell configuration was used to decouple the voltage contributions from the graphite anode and the intercalated cathode. The equivalent circuit and the electrochemical mechanism of the iR drop method are illustrated in Fig. 14a. The change in electrode potential is defined as iR drop. Upon application of a current pulse signal, the polarization, which can be divided into electrochemical polarization and concentration polarization, occurs at the electrode thereby causing a change in the electrode voltage. Charge transfer can be stopped by terminating the application of current, and thus

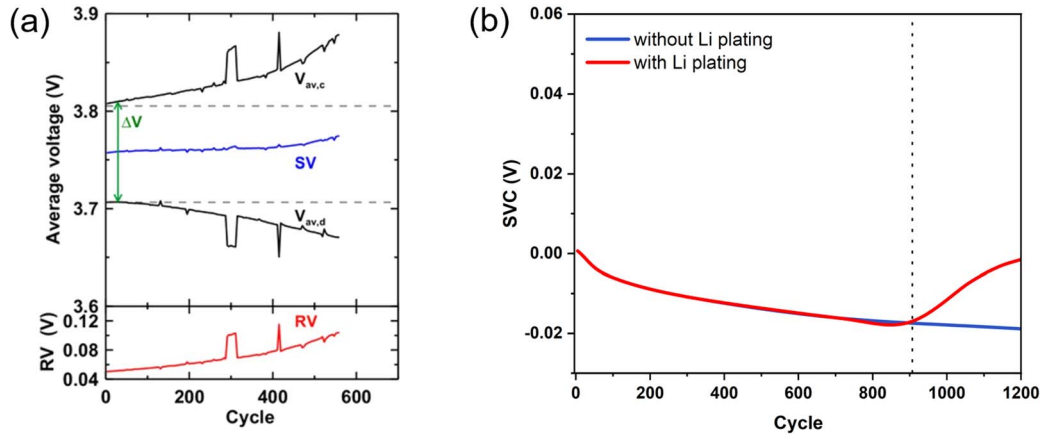

Fig. 13 (a) Average voltages indicated with solid black lines. The dashed lines indicate a perfect cell with an unchanging average voltage. The blue line represents the value of SV and the red line represents the value of RV. (b) Variation of SVC with the number of cycles. Reproduced under terms of the CC-BY license.[152] Copyright 2018, The Authors, published by ECS.

the electrochemical polarization will disappear, resulting in a significant drop in voltage. A three-electrode configuration was used to assemble the cell so that the iR drop could be obtained for the cathode and anode, respectively, as shown in Fig. 14b. The iR drop of the graphite electrode was used for the study and defined as R_i, which was charged and discharged at different C rates. When the C rate is large enough for lithium plating to occur, the trend of R_i is always decreasing followed by

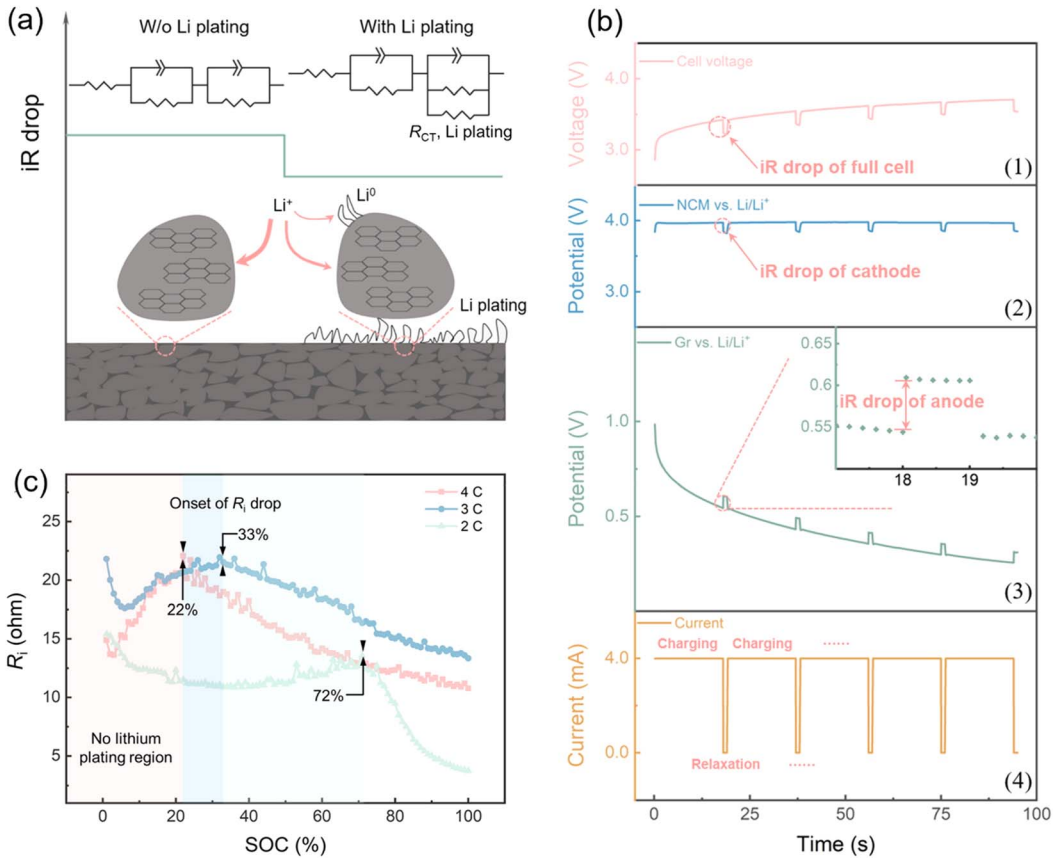

Fig. 14 (a) Schematic illustration of the detection mechanism of lithium plating by iR drop; (b) charging protocol for detecting the onset of lithium plating in a three-electrode cell configuration: voltage profile of (1) the full cell, (2) $LiNi_{0.5}Co_{0.2}Mn_{0.3}O_2$ cathode, and (3) graphite anode, inset in (3) is the iR drop calculated from the anode potential. (4) Current profile of the full cell. (c) R_i from iR drop at 2C, 3C, and 4C charging; the sharp decrease points to the onset of lithium plating. Reproduced under terms of the CC-BY license.[153] Copyright, 2021 Science Press and Dalian Institute of Chemical Physics, Chinese Academy of Sciences, published by Elsevier.

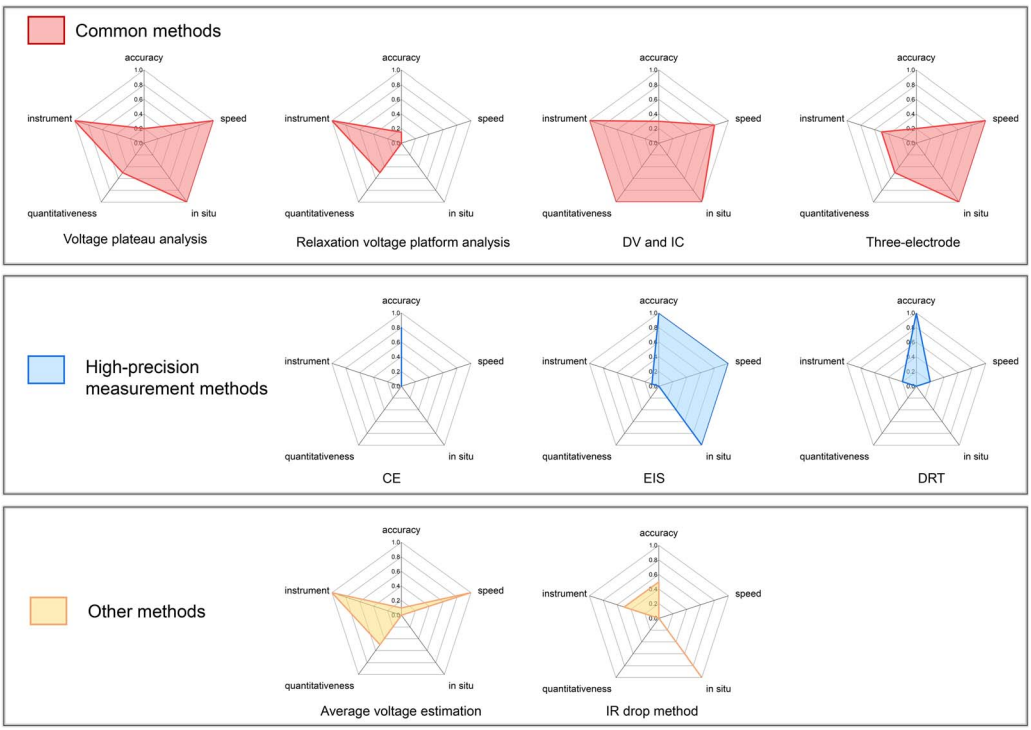

Fig. 15 Comparison of different electrochemical methods for lithium plating detection.

increasing and then decreasing. The second beginning of the curve's attenuation was regarded as the beginning of lithium plating. The authors compared the point marking the second start of the decline of R_i with Fear's work[118] and found consistency between their conclusions, and verified the reliability of the iR pressure drop method by observing the lithium plating with a light microscope.

Although the iR drop method is relatively easy to operate and only needs to stop the discharging process continuously to get the results, this operation needs to be repeated many times in

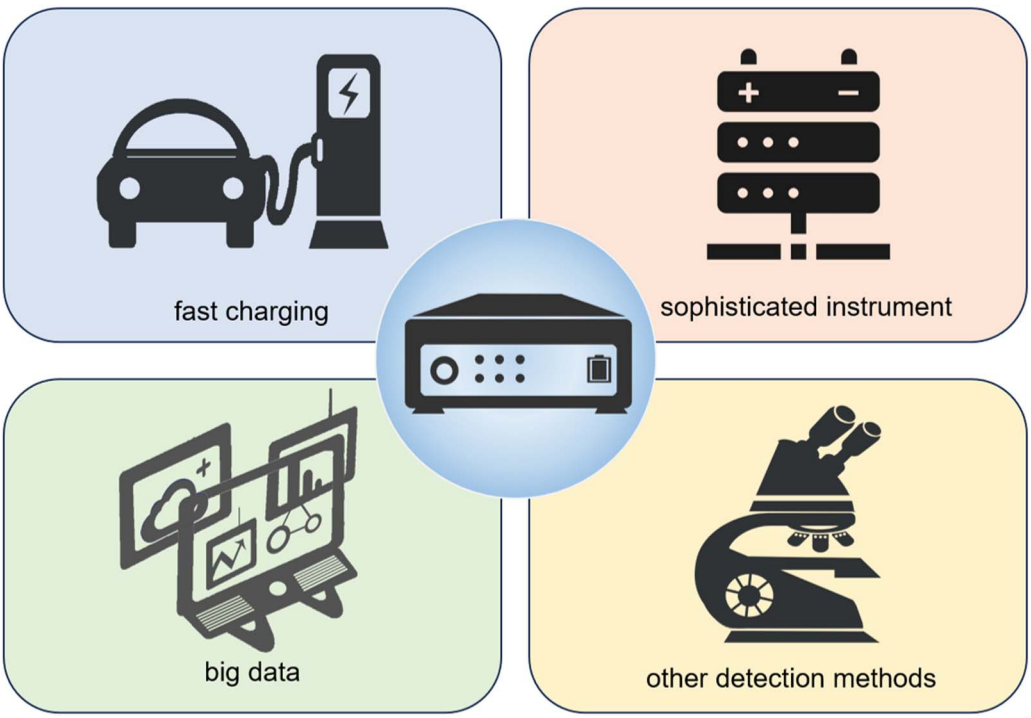

Fig. 16 Prospects of electrochemical detection methods for lithium plating.

order to obtain a continuous iR drop curve. In addition, the iR drop is recorded by disconnecting every 1% SOC, and the number of iR drop data to be recorded is very complicated, which is unlikely to occur in practical applications. Moreover, the nature of using the iR drop method is the measurement of charge transfer impedance, which cannot detect the impedance of lithium-ions through the SEI layer as opposed to the traditional direct measurement of EIS.

4 Summary and outlook

The major challenge for fast charging is lithium plating on the graphite anode, which not only triggers safety issues but also leads to the degradation of LIBs. Therefore, the observation and analysis methods of lithium plating are very necessary to be studied. The key to electrochemical detection is to relate the lithium plating behavior to the change in the electrochemical performance of the battery during the cycle. This review first analyzes the formation mechanism of lithium plating and briefly summarizes the current research related to the detection method from the perspective of electrochemical methods. Each method has its own merits and drawbacks. Fig. 15 provides a comparison between different methods, allowing for the selection of an appropriate detection method tailored to specific testing needs in order to achieve better detection of lithium plating. And in order to further understand lithium plating and realize real-time detection of this side reaction, some prospects for further research are proposed (Fig. 16).

(1) Currently, no electrochemical method can reliably and accurately detect the onset of lithium plating while the battery is charging. The commonly used electrochemical methods are based on the stripping platform during discharging or the voltage platform during relaxation. So it is not possible to take measures to stop lithium plating from continuing when it occurs. This is obviously very unfavorable for preventing the occurrence of lithium plating in the actual practical application of LIBs. If lithium plating has occurred in the battery, even if it is detected during the process after charging, the harm caused by lithium plating is irreversible. Therefore, it is very important to develop reliable means to indicate the occurrence of lithium plating during the charging process. Additionally, some impedance-based detection methods exhibit extremely high sensitivity at room temperature. When combined with big data technologies, they can be effectively applied to detect lithium plating in vehicle-mounted batteries.[21]

(2) In order to improve the accuracy of lithium plating detection by an electrochemical method, it is necessary to improve the accuracy of the original data. However, obtaining highly accurate data for the hardware and software of the instrument is a great challenge. Therefore, the development of more sophisticated instruments is an urgent priority. Only then can we more accurately understand the small changes in the measurement.

(3) Many electrochemical detection methods can be combined with big data technologies, such as cloud-based BMSs that offer promising utilization for real-time monitoring of lithium plating *via* embedded sensors such as reference electrodes. Combining big data techniques and model-based approaches, advanced algorithms can further predict and avoid lithium plating. Detecting lithium plating is a complex task. By gaining a deeper understanding of the lithium plating mechanism under different operating conditions and applying advanced detection methods, we can significantly reduce degradation under extreme circumstances and achieve a longer cycle life.

(4) The lithium plating on the surface of the graphite electrode is specific, which means that the lithium plating state of the same battery is different at different locations. However, these specific changes cannot be detected by a single electrochemical method. In order to better obtain localized information on lithium plating, it is necessary to combine various high-end characterization techniques to jointly perform lithium analysis and improve the accuracy of detection, such as scanning electron microscopy, *in situ* optical microscopy, *in situ* transmission electron microscopy, and so on.

Data availability

The data analyzed here are available from the original experimental studies referenced.

Conflicts of interest

The authors declare no conflict of interest.

Acknowledgements

This work was supported by the National Science Foundation of Sichuan Province (No. 2023NSFSC1124), Fundamental Research Funds for the Central Universities (No. YJ2021141), the Science and Technology Cooperation Special Fund of Sichuan University and Zigong City (No. 2022CDZG-9), and the Foundation of Key Laboratory for Palygorskite Science and Applied Technology of Jiangsu Province (No. HPK202303).

References

1 T. Gao, Y. Han, D. Fraggedakis, S. Das, T. Zhou, C.-N. Yeh, S. Xu, W. C. Chueh, J. Li and M. Z. Bazant, *Joule*, 2021, **5**, 393–414.
2 X. Zhang, A. Han and Y. Yang, *J. Mater. Chem. A*, 2020, **8**, 22455–22466.
3 J. Gong, C. Li and M. R. Wasielewski, *Chem. Soc. Rev.*, 2019, **48**, 1862–1864.
4 S. Jin, X. Gao, S. Hong, Y. Deng, P. Chen, R. Yang, Y. L. Joo and L. A. Archer, *Joule*, 2024, **8**, 746–763.
5 G. Li, Z. Yang, Z. Yin, H. Guo, Z. Wang, G. Yan, Y. Liu, L. Li and J. Wang, *J. Mater. Chem. A*, 2019, **7**, 15541–15563.
6 M. Tian, Y. Yan, H. Yu, L. Ben, Z. Song, Z. Jin, G. Cen, J. Zhu, M. Armand, H. Zhang, Z. Zhou and X. Huang, *Adv. Mater.*, 2024, **36**, 2400707.
7 T. Xu, X. Ding, H. Cheng, G. Han and L. Qu, *Adv. Mater.*, 2023, **36**, 2209661.

8 N. Chen, H. Zhang, L. Li, R. Chen and S. Guo, *Adv. Energy Mater.*, 2018, **8**, 1702675.
9 Z. Li, Y.-X. Yao, M. Zheng, S. Sun, Y. Yang, Y. Xiao, L. Xu, C.-B. Jin, X.-Y. Yue, T. Song, P. Wu, C. Yan and Q. Zhang, *Angew. Chem., Int. Ed.*, 2024, e202409409.
10 Z. Li, N. Yao, L. Yu, Y.-X. Yao, C.-B. Jin, Y. Yang, Y. Xiao, X.-Y. Yue, W.-L. Cai, L. Xu, P. Wu, C. Yan and Q. Zhang, *Matter*, 2023, **6**, 2274–2292.
11 P. M. Attia, A. Bills, F. Brosa Planella, P. Dechent, G. dos Reis, M. Dubarry, P. Gasper, R. Gilchrist, S. Greenbank, D. Howey, O. Liu, E. Khoo, Y. Preger, A. Soni, S. Sripad, A. G. Stefanopoulou and V. Sulzer, *J. Electrochem. Soc.*, 2022, **169**, 060517.
12 Z. Li, Z. Wu, S. Wu, W. Tang, J. Qiu, T. Liu, Z. Lin and J. Lu, *Adv. Funct. Mater.*, 2024, **34**, 2307261.
13 Y. Yan, T. Zeng, S. Liu, C. Z. Shu and Y. Zeng, *Energy Mater.*, 2023, **3**, 300003.
14 K. Zhang, C. Zhang, L. Wu, Q. Yang, J. Zhang, G. Hu, L. Song, G. Li and W. Cai, *Chin. Chem. Lett.*, 2024, **35**, 109618.
15 Z. Li, Y.-X. Yao, S. Sun, C.-B. Jin, N. Yao, C. Yan and Q. Zhang, *Angew. Chem., Int. Ed.*, 2023, **62**, e202303888.
16 Z. Dobó, T. Dinh and T. Kulcsár, *Energy Rep.*, 2023, **9**, 6362–6395.
17 P. Wang, J.-H. Liu, W. Cui, X. Li, Z. Li, Y. Wan, J. Zhang and Y.-Z. Long, *J. Mater. Chem. A*, 2023, **11**, 16539–16558.
18 Y.-J. Liu, R.-Y. Fang and D. Mitlin, *Tungsten*, 2022, **4**, 316–322.
19 L. H. J. Raijmakers, D. L. Danilov, R. A. Eichel and P. H. L. Notten, *Appl. Energ.*, 2019, **240**, 918–945.
20 N. Lingappan, W. Lee, S. Passerini and M. Pecht, *Renewable Sustainable Energy Rev.*, 2023, **187**, 113726.
21 U. R. Koleti, T. Q. Dinh and J. Marco, *J. Power Sources*, 2020, **451**, 227798.
22 Z. Li, G. Wu, Y. Yang, Z. Wan, X. Zeng, L. Yan, S. Wu, M. Ling, C. Liang, K. N. Hui and Z. Lin, *Adv. Energy Mater.*, 2022, **12**, 2201197.
23 X.-L. Gao, X.-H. Liu, W.-L. Xie, L.-S. Zhang and S.-C. Yang, *Rare Met.*, 2021, **40**, 3038–3048.
24 P. V. Chombo and Y. Laoonual, *J. Power Sources*, 2020, **478**, 228649.
25 Y. Yan, T. Zeng, S. Liu, C. Z. Shu and Y. Zeng, *Energy Mater.*, 2023, **35**, 2206625.
26 X. Feng, M. Ouyang, X. Liu, L. Lu, Y. Xia and X. He, *Energy Storage Mater.*, 2018, **10**, 246–267.
27 L. Cai-Cai, Z. Xu-Sheng, Z. Yu-Hui, Z. Ying, X. Sen, W. Li-Jun and G. Yu-Guo, *Energy Mater.*, 2021, **1**, 100017.
28 X. Zhang, Z. Li, L. Luo, Y. Fan and Z. Du, *Energy*, 2022, **238**, 121652.
29 Q. Huang, S. Ni, M. Jiao, X. Zhong, G. Zhou and H.-M. Cheng, *Small*, 2021, **17**, 2007676.
30 Y. Sun, Y. Jin, Z. Jiang and L. Li, *Eng. Failure Anal.*, 2023, **149**, 107259.
31 Z. Li, Z. Wan, X. Zeng, S. Zhang, L. Yan, J. Ji, H. Wang, Q. Ma, T. Liu, Z. Lin, M. Ling and C. Liang, *Nano Energy*, 2021, **79**, 105430.
32 S. Zeng, X. Zhou, B. Wang, Y. Feng, R. Xu, H. Zhang, S. Peng and Y. Yu, *J. Mater. Chem. A*, 2019, **7**, 15774–15781.
33 Y. Wang, Z. Wang, Y. Chen, H. Zhang, M. Yousaf, H. Wu, M. Zou, A. Cao and R. P. S. Han, *Adv. Mater.*, 2018, **30**, 1802074.
34 C. Meng, M. Yuan, B. Cao, X. Lin, J. Zhang, A. Li, X. Chen, M. Jia and H. Song, *Carbon*, 2022, **192**, 347–355.
35 S. Komaba, T. Ozeki and K. Okushi, *J. Power Sources*, 2009, **189**, 197–203.
36 K. Chen, H. Yang, F. Liang and D. Xue, *ACS Appl. Mater. Interfaces*, 2018, **10**, 909–914.
37 T. H. N. G. Amaraweera, N. W. B. Balasooriya, H. W. M. A. C. Wijayasinghe, A. N. B. Attanayake, B. E. Mellander and M. A. K. L. Dissanayake, *Ionics*, 2018, **24**, 3423–3429.
38 S. Yang, K. Yamamoto, X. Mei, A. Sakuda, T. Uchiyama, T. Watanabe, T. Takami, A. Hayashi, M. Tatsumisago and Y. Uchimoto, *ACS Appl. Energy Mater.*, 2022, **5**, 667–673.
39 P. Zhuo, J. Jiang, Y. Jiang, Y. Hao, Q. He, T. Chen, E. Ding, Y. Zhang, Y. Han, W. Si, Z. Ju, Y. Cao, Y. Xing, X. Gui and J. Colloid Interf, *Sci*, 2023, **648**, 108–116.
40 W. Guoping, Z. Bolan, Y. Min, X. Xiaoluo, Q. Meizheng and Y. Zuolong, *Solid State Ionics*, 2005, **176**, 905–909.
41 Z. Li, R. Fang, H. Ge, Z. Liu, F. B. Spingler, A. Jossen, J. Zhang and B. Liaw, *J. Electrochem. Soc.*, 2022, **169**, 080530.
42 M.-T. F. Rodrigues, K. Kalaga, S. E. Trask, D. W. Dees, I. A. Shkrob and D. P. Abraham, *J. Electrochem. Soc.*, 2019, **166**, A996.
43 M.-T. F. Rodrigues, I. A. Shkrob, A. M. Colclasure and D. P. Abraham, *J. Electrochem. Soc.*, 2020, **167**, 130508.
44 I. A. Shkrob, M.-T. F. Rodrigues and D. P. Abraham, *J. Electrochem. Soc.*, 2021, **168**, 010512.
45 U. Janakiraman, T. R. Garrick and M. E. Fortier, *J. Electrochem. Soc.*, 2020, **167**, 160552.
46 S. Schindler, M. Bauer, M. Petzl and M. A. Danzer, *J. Power Sources*, 2016, **304**, 170–180.
47 D. Ren, H. Hsu, R. Li, X. Feng, D. Guo, X. Han, L. Lu, X. He, S. Gao, J. Hou, Y. Li, Y. Wang and M. Ouyang, *eTransportation*, 2019, **2**, 100034.
48 Y. Yamada, K. Furukawa, K. Sodeyama, K. Kikuchi, M. Yaegashi, Y. Tateyama and A. Yamada, *J. Am. Chem. Soc.*, 2014, **136**, 5039–5046.
49 W. Mei, L. Jiang, H. J. Zhou, J. Sun and Q. Wang, *J. Energy Chem.*, 2022, **74**, 446–453.
50 P. Li, C. Li, Y. Yang, C. Zhang, R. Wang, Y. Liu, Y. Wang, J. Luo, X. Dong and Y. Xia, *Research*, 2019, **2019**, 7481319.
51 R. Wang, X. Li, Z. Wang and H. Zhang, *Nano Energy*, 2017, **34**, 131–140.
52 A. Klein, M. Sadd, N. Mozhzhukhina, M. Olsson, L. Broche, S. Xiong and A. Matic, *Batteries Supercaps*, 2024, **7**, e202400070.
53 W. Cai, C. Yan, Y.-X. Yao, L. Xu, R. Xu, L.-L. Jiang, J.-Q. Huang and Q. Zhang, *Small Struct.*, 2020, **1**, 2000010.
54 Y. Wen, K. He, Y. Zhu, F. Han, Y. Xu, I. Matsuda, Y. Ishii, J. Cumings and C. Wang, *Nat. Commun.*, 2014, **5**, 4033.

55 W. Cai, Y.-X. Yao, G.-L. Zhu, C. Yan, L.-L. Jiang, C. He, J.-Q. Huang and Q. Zhang, *Chem. Soc. Rev.*, 2020, **49**, 3806–3833.
56 K. Shen, J. Dai, Y. Zheng, C. Xu, R. Zhang, H. Wang, C. Jin, X. Han, X. Lai, X. Qian and X. Feng, *Therm. Sci. Eng. Prog.*, 2023, **46**, 102197.
57 Y. T. Jeong, H. R. Shin, J. Lee, M.-H. Ryu, S. Choi, H. Kim, K.-N. Jung and J.-W. Lee, *Electrochim. Acta*, 2023, **462**, 142761.
58 Y. Qin, P. Zuo, X. Chen, W. Yuan, R. Huang, X. Yang, J. Du, L. Lu, X. Han and M. Ouyang, *J. Energy Chem.*, 2022, **72**, 442–452.
59 H. Yu, L. Yang, L. Zhang, J. Li and X. Liu, *iScience*, 2022, **25**, 104243.
60 J. Liu, Z. Chu, H. Li, D. Ren, Y. Zheng, L. Lu, X. Han and M. Ouyang, *Int. J. Energy Res.*, 2021, **45**, 7918–7932.
61 D. Lee, B. Kim and C. B. Shin, *J. Electrochem. Soc.*, 2022, **169**, 090502.
62 W. Cai, C. Yan, Y. X. Yao, L. Xu, X. R. Chen, J. Q. Huang and Q. Zhang, *Angew. Chem., Int. Ed.*, 2021, **60**, 13007–13012.
63 X. Xu, X. Yue, Y. Chen and Z. Liang, *Angew. Chem., Int. Ed.*, 2023, **62**, e202306963.
64 N. Ghanbari, T. Waldmann, M. Kasper, P. Axmann and M. Wohlfahrt-Mehrens, *ECS Electrochem. Lett.*, 2015, **4**, A100.
65 P. P. Paul, E. J. McShane, A. M. Colclasure, N. Balsara, D. E. Brown, C. Cao, B.-R. Chen, P. R. Chinnam, Y. Cui, E. J. Dufek, D. P. Finegan, S. Gillard, W. Huang, Z. M. Konz, R. Kostecki, F. Liu, S. Lubner, R. Prasher, M. B. Preefer, J. Qian, M.-T. F. Rodrigues, M. Schnabel, S.-B. Son, V. Srinivasan, H.-G. Steinrück, T. R. Tanim, M. F. Toney, W. Tong, F. Usseglio-Viretta, J. Wan, M. Yusuf, B. D. McCloskey and J. Nelson Weker, *Adv. Energy Mater.*, 2021, **11**, 2100372.
66 X. Liu, L. Zhang, H. Yu, J. Wang, J. Li, K. Yang, Y. Zhao, H. Wang, B. Wu, N. P. Brandon and S. Yang, *Adv. Energy Mater.*, 2022, **12**, 2200889.
67 H. Ge, T. Aoki, N. Ikeda, S. Suga, T. Isobe, Z. Li, Y. Tabuchi and J. Zhang, *J. Electrochem. Soc.*, 2017, **164**, A1050.
68 E. J. McShane, A. M. Colclasure, D. E. Brown, Z. M. Konz, K. Smith, B. D. McCloskey and B. D. McCloskey, *ACS Energy Lett.*, 2020, **5**, 2045–2051.
69 F. Grimsmann, T. Gerbert, F. Brauchle, A. Gruhle, J. Parisi and M. Knipper, *J. Power Sources*, 2017, **365**, 12–16.
70 B. Bitzer and A. Gruhle, *J. Power Sources*, 2014, **262**, 297–302.
71 C. von Lüders, V. Zinth, S. V. Erhard, P. J. Osswald, M. Hofmann, R. Gilles and A. Jossen, *J. Power Sources*, 2017, **342**, 17–23.
72 M. T. M. Pham, J. J. Darst, D. P. Finegan, J. B. Robinson, T. M. M. Heenan, M. D. R. Kok, F. Iacoviello, R. Owen, W. Q. Walker, O. V. Magdysyuk, T. Connolley, E. Darcy, G. Hinds, D. J. L. Brett and P. R. Shearing, *J. Power Sources*, 2020, **470**, 228039.
73 F. Sun, L. Zielke, H. Markötter, A. Hilger, D. Zhou, R. Moroni, R. Zengerle, S. Thiele, J. Banhart and I. Manke, *ACS Nano*, 2016, **10**, 7990–7997.
74 A. S. Ho, D. Y. Parkinson, D. P. Finegan, S. E. Trask, A. N. Jansen, W. Tong and N. P. Balsara, *ACS Nano*, 2021, **15**, 10480–10487.
75 L. E. Downie, L. J. Krause, J. C. Burns, L. D. Jensen, V. L. Chevrier and J. R. Dahn, *J. Electrochem. Soc.*, 2013, **160**, A588.
76 M. Fleischhammer, T. Waldmann, G. Bisle, B.-I. Hogg and M. Wohlfahrt-Mehrens, *J. Power Sources*, 2015, **274**, 432–439.
77 H. Xu, C. Han, W. Li, H. Li and X. Qiu, *J. Power Sources*, 2022, **529**, 231219.
78 Y. Tian, C. Lin, H. Li, J. Du and R. Xiong, *Appl. Energ.*, 2021, **300**, 117386.
79 S. Goriparti, E. Miele, F. De Angelis, E. Di Fabrizio, R. Proietti Zaccaria and C. Capiglia, *J. Power Sources*, 2014, **257**, 421–443.
80 W. Mei, L. Jiang, C. Liang, J. Sun and Q. Wang, *Energy Storage Mater.*, 2021, **41**, 209–221.
81 Y. Sun, G. Zheng, Z. W. Seh, N. Liu, S. Wang, J. Sun, H. R. Lee and Y. Cui, *Chem*, 2016, **1**, 287–297.
82 N. Legrand, B. Knosp, P. Desprez, F. Lapicque and S. Raël, *J. Power Sources*, 2014, **245**, 208–216.
83 P. Keil and A. Jossen, *J. Energy Storage*, 2016, **6**, 125–141.
84 S. P. Rangarajan, C. Fear, T. Adhikary, Y. Barsukov, G. Dadheech and P. P. Mukherjee, *Cell Rep. Phys. Sci.*, 2023, **4**, 101740.
85 T. Waldmann, M. Kasper and M. Wohlfahrt-Mehrens, *Electrochim. Acta*, 2015, **178**, 525–532.
86 Y. Xiong, Y. Liu, L. Chen, S. Zhang, X. Zhu, T. Shen, D. Ren, X. He, J. Qiu, L. Wang, Q. Hu and H. Zhang, *Energy Environ. Mater.*, 2022, **5**, 872–876.
87 G. Zhang, X. Wei, G. Han, H. Dai, J. Zhu, X. Wang, X. Tang and J. Ye, *J. Power Sources*, 2021, **484**, 229312.
88 K. Sun, X. Li, Z. Zhang, X. Xiao, L. Gong and P. Tan, *ACS Appl. Mater. Interfaces*, 2023, **15**, 36356–36365.
89 M. Ecker, P. Shafiei Sabet and D. U. Sauer, *Appl. Energy*, 2017, **206**, 934–946.
90 M. M. Forouzan, S. Khaleghi Rahimian, S. Han, Y. Liu and Y. Tang, *ECS Meeting Abstracts*, 2019, **MA2019-01**, 394.
91 X.-G. Yang and C.-Y. Wang, *J. Power Sources*, 2018, **402**, 489–498.
92 H. Liu, X. B. Cheng, R. Xu, X. Q. Zhang, C. Yan, J. Q. Huang and Q. Zhang, *Adv. Energy Mater.*, 2019, **9**, 1902254.
93 D. Ren, K. Smith, D. Guo, X. Han, X. Feng, L. Lu, M. Ouyang and J. Li, *J. Electrochem. Soc.*, 2018, **165**, A2167–A2178.
94 T. Gao, Y. Han, D. Fraggedakis, S. Das, T. Zhou, C.-N. Yeh, S. Xu, W. C. Chueh, J. Li and M. Z. Bazant, *Joule*, 2021, **5**, 393–414.
95 C. Uhlmann, J. Illig, M. Ender, R. Schuster and E. Ivers-Tiffée, *J. Power Sources*, 2015, **279**, 428–438.
96 J. F. Ding, R. Xu, X. X. Ma, Y. Xiao, Y. X. Yao, C. Yan and J. Q. Huang, *Angew. Chem., Int. Ed.*, 2022, **61**, e202115602.
97 X. Duan, B. Li, J. Li, X. Gao, L. Wang and J. Xu, *Adv. Energy Mater.*, 2023, **13**, 2203767.
98 D. Han and C. Lin, *J. Energy Storage*, 2024, **83**, 110641.
99 X. Gao, Y.-N. Zhou, D. Han, J. Zhou, D. Zhou, W. Tang and J. B. Goodenough, *Joule*, 2020, **4**, 1864–1879.

100 B. S. Vishnugopi and P. P. Mukherjee, *Joule*, 2022, **6**, 291–293.
101 D. Wang, W. Zhang, W. Zheng, X. Cui, T. Rojo and Q. Zhang, *Adv. Sci.*, 2016, **4**, 1600168.
102 Y. Zhang, C. Wang, G. Pastel, Y. Kuang, H. Xie, Y. Li, B. Liu, W. Luo, C. Chen and L. Hu, *Adv. Energy Mater.*, 2018, **8**, 1800635.
103 Y. Jeoun, K. Kim, S.-Y. Kim, S.-H. Lee, S.-H. Huh, S. H. Kim, X. Huang, Y.-E. Sung, H. D. Abruña and S.-H. Yu, *ACS Energy Lett.*, 2022, **7**, 2219–2227.
104 C. Jin, T. Liu, O. Sheng, M. Li, T. Liu, Y. Yuan, J. Nai, Z. Ju, W. Zhang, Y. Liu, Y. Wang, Z. Lin, J. Lu and X. Tao, *Nat. Energy*, 2021, **6**, 378–387.
105 M. Li, J. Lu, Z. Chen and K. Amine, *Adv. Mater.*, 2018, **30**, 1800561.
106 Y. Liu, Y. Li, L. Chen, F. Yan, Z. Lin, J. Wang, J. Qiu, G. Cao, B. Wang and H. Zhang, *Energy Storage Mater.*, 2022, **53**, 621–628.
107 S.-C. Miao, Y. Jia, Z.-W. Deng, Y. Deng, R.-X. Chen, X.-M. Zhang, C.-H. Xu, M. Yao and W.-L. Cai, *Tungsten*, 2023, **6**, 212–229.
108 W. Huang, Y. Ye, H. Chen, R. A. Vilá, A. Xiang, H. Wang, F. Liu, Z. Yu, J. Xu, Z. Zhang, R. Xu, Y. Wu, L.-Y. Chou, H. Wang, J. Xu, D. T. Boyle, Y. Li and Y. Cui, *Nat. Commun.*, 2022, **13**, 7091.
109 Y. Huang, D. Perlmutter, A. Fei-Huei Su, J. Quenum, P. Shevchenko, D. Y. Parkinson, I. V. Zenyuk and D. Ushizima, *npj Compu. Mater*, 2023, **9**, 93.
110 A. Straßer, A. Adam and J. Li, *J. Power Sources*, 2023, **580**, 233366.
111 H. You, B. Jiang, J. Zhu, X. Wang, G. Shi, G. Han, X. Wei and H. Dai, *J. Power Sources*, 2023, **564**, 232892.
112 S. Zhang, Z. Wei, L. Zhang, J. Hu and R. Dai, *J. Power Sources*, 2024, **600**, 234239.
113 Y. Chen, L. Torres-Castro, K.-H. Chen, D. Penley, J. Lamb, M. Karulkar and N. P. Dasgupta, *J. Power Sources*, 2022, **539**, 231601.
114 M. C. Smart and B. V. Ratnakumar, *J. Electrochem. Soc.*, 2011, **158**, A379.
115 M. Petzl and M. A. Danzer, *J. Power Sources*, 2014, **254**, 80–87.
116 W. Mei, Y. Zhang, Y. Li, P. Zhuo, Y. Chu, Y. Chen, L. Jiang, H. Zhou, J. Sun and Q. Wang, *Energy Storage Mater.*, 2024, **66**, 103193.
117 X.-G. Yang, S. Ge, T. Liu, Y. Leng and C.-Y. Wang, *J. Power Sources*, 2018, **395**, 251–261.
118 C. Fear, T. Adhikary, R. Carter, A. N. Mistry, C. T. Love and P. P. Mukherjee, *ACS Appl. Mater. Interfaces*, 2020, **12**, 30438–30448.
119 J. Sieg, M. Storch, J. Fath, A. Nuhic, J. Bandlow, B. Spier and D. U. Sauer, *J. Energy Storage*, 2020, **30**, 101582.
120 M. Petzl, M. Kasper and M. A. Danzer, *J. Power Sources*, 2015, **275**, 799–807.
121 I. D. Campbell, M. Marzook, M. Marinescu and G. J. Offer, *J. Electrochem. Soc.*, 2019, **166**, A725.
122 M. Lewerenz, A. Marongiu, A. Warnecke and D. U. Sauer, *J. Power Sources*, 2017, **368**, 57–67.
123 M. Dubarry, V. Svoboda, R. Hwu and B. Yann Liaw, *Electrochem. Solid-State Lett.*, 2006, **9**, A454.
124 M. Dubarry and B. Y. Liaw, *J. Power Sources*, 2009, **194**, 541–549.
125 M. Dubarry, C. Truchot, B. Y. Liaw, K. Gering, S. Sazhin, D. Jamison and C. Michelbacher, *J. Power Sources*, 2011, **196**, 10336–10343.
126 C. Pastor-Fernández, K. Uddin, G. H. Chouchelamane, W. D. Widanage and J. Marco, *J. Power Sources*, 2017, **360**, 301–318.
127 D. Anseán, M. Dubarry, A. Devie, B. Y. Liaw, V. M. García, J. C. Viera and M. González, *J. Power Sources*, 2017, **356**, 36–46.
128 I. Bloom, A. N. Jansen, D. P. Abraham, J. Knuth, S. A. Jones, V. S. Battaglia and G. L. Henriksen, *J. Power Sources*, 2005, **139**, 295–303.
129 Y. Li, M. Abdel-Monem, R. Gopalakrishnan, M. Berecibar, E. Nanini-Maury, N. Omar, P. van den Bossche and J. Van Mierlo, *J. Power Sources*, 2018, **373**, 40–53.
130 D. Ren, K. Smith, D. Guo, X. Han, X. Feng, L. Lu, M. Ouyang and J. Li, *J. Electrochem. Soc.*, 2018, **165**, A2167.
131 R. Drees, J. Herdegen, F. Lienesch and M. Kurrat, *J. Power Sources*, 2024, **594**, 233986.
132 Y. Zhang and C.-Y. Wang, *J. Electrochem. Soc.*, 2009, **156**, A527.
133 T. Waldmann, B. I. Hogg, M. Kasper, S. Grolleau, C. G. Couceiro, K. Trad, B. P. Matadi and M. Wohlfahrt-Mehrens, *J. Electrochem. Soc.*, 2016, **163**, A1232–A1238.
134 J. Zhou and P. H. L. Notten, *J. Electrochem. Soc.*, 2004, **151**, A2173.
135 S. Solchenbach, D. Pritzl, E. J. Y. Kong, J. Landesfeind and H. A. Gasteiger, *J. Electrochem. Soc.*, 2016, **163**, A2265–A2272.
136 S. Yi, B. Wang, Z. Chen, R. Wang and D. Wang, *RSC Adv.*, 2018, **8**, 18597–18603.
137 D. P. Abraham, S. D. Poppen, A. N. Jansen, J. Liu and D. W. Dees, *Electrochim. Acta*, 2004, **49**, 4763–4775.
138 D. W. Dees, A. N. Jansen and D. P. Abraham, *J. Power Sources*, 2007, **174**, 1001–1006.
139 S. S. Zhang, K. Xu and T. R. Jow, *J. Power Sources*, 2006, **160**, 1349–1354.
140 J. C. Burns, D. A. Stevens and J. R. Dahn, *J. Electrochem. Soc.*, 2015, **162**, A959.
141 Y. Pan, D. Ren, X. Han, L. Lu and M. Ouyang, *Batteries*, 2022, **8**, 206.
142 D. E. Brown, E. J. McShane, Z. M. Konz, K. B. Knudsen and B. D. McCloskey, *Cell Rep. Phys. Sci.*, 2021, **2**, 100589.
143 M. Koseoglou, E. Tsioumas, D. Ferentinou, N. Jabbour, D. Papagiannis and C. Mademlis, *J. Power Sources*, 2021, **512**, 230508.
144 L. Xu, Y. Xiao, Y. Yang, S.-J. Yang, X.-R. Chen, R. Xu, Y.-X. Yao, W.-L. Cai, C. Yan, J.-Q. Huang and Q. Zhang, *Angew. Chem., Int. Ed.*, 2022, **61**, e202210365.
145 J. Illig, M. Ender, T. Chrobak, J. P. Schmidt, D. Klotz and E. Ivers-Tiffée, *J. Electrochem. Soc.*, 2012, **159**, A952–A960.
146 H. Schichlein, A. C. Müller, M. Voigts, A. Krügel and E. Ivers-Tiffée, *J. Appl. Electrochem.*, 2002, **32**, 875–882.

147 A. L. Smirnova, K. R. Ellwood and G. M. Crosbie, *J. Electrochem. Soc.*, 2001, **148**, A610–A615.
148 X. Chen, L. Li, M. Liu, T. Huang and A. Yu, *J. Power Sources*, 2021, **496**, 229867.
149 N. Harting, N. Wolff, F. Röder and U. Krewer, *Electrochim. Acta*, 2017, **248**, 133–139.
150 N. Harting, N. Wolff and U. Krewer, *Electrochim. Acta*, 2018, **281**, 378–385.
151 M. D. Murbach and D. T. Schwartz, *J. Electrochem. Soc.*, 2017, **164**, E3311.
152 J. E. Harlow, S. L. Glazier, J. Li and J. R. Dahn, *J. Electrochem. Soc.*, 2018, **165**, A3595.
153 L. Xu, Y. Yang, Y. Xiao, W.-L. Cai, Y.-X. Yao, X.-R. Chen, C. Yan, H. Yuan and J.-Q. Huang, *J. Energy Chem.*, 2022, **67**, 255–262.